## Original Article

**CAMBRIDGE**
UNIVERSITY PRESS

# Natural fractures in tight gas sandstones: a case study of the Upper Triassic Xujiahe Formation in Xinchang gas field, Western Sichuan Basin, China

Yunzhao Zhang[1,2] , Lianbo Zeng[1,2], Wenya Lyu[1,2], Dongsheng Sun[3], Shuangquan Chen[1], Cong Guan[1,2], Lei Tang[2,4], Jinxiong Shi[5] and Junhui Zhang[6]

[1]State Key Laboratory of Petroleum Resources and Prospecting, China University of Petroleum (Beijing), Beijing, 102249, China; [2]College of Geosciences, China University of Petroleum (Beijing), Beijing, 102249, China; [3]Petroleum Exploration and Production Research Institute, Sinopec, Beijing, 100083, China; [4]Geophysical Exploration Institute, Jiangsu Oilfield, Sinopec, Nanjing, 210046, China; [5]School of Geosciences, Yangtze University, Wuhan, 434100, China and [6]Research Institute of Exploration and Development of Sinopec Southwest Oil and Gas Company, Deyang, 618000, China

## Abstract

The Upper Triassic Xujiahe Formation is a typical tight gas reservoir in which natural fractures determine the migration, accumulation and production capacity of tight gas. In this study, we focused on the influences of natural fractures on the tight gas migration and production. We clarified characteristics and attributes (i.e. dips, apertures, filling degree and cross-cutting relationships) of the fractures based on image logging interpretations and core descriptions. Previous studies of electron spin resonance, carbon and oxygen isotopes, homogenization temperature of fluid inclusions analysis and basin simulation were considered. This study also analysed the fracture sequences, source of fracture fillings, diagenetic sequences and tight gas enrichment stages. We obtained insight into the relationship between fracture evolution and hydrocarbon charging, particularly the effect of the apertures and intensity of natural fractures on tight gas production. We reveal that the bedding fractures are short horizontal migration channels of tight gas. The tectonic fractures with middle, high and nearly vertical angles are beneficial to tight gas vertical migration. The apertures of fractures are controlled by the direction of maximum principal stress and fracture angle. The initial gas production of the vertical wells presents a positive correlation with the fracture abundance, and the intensity and aperture of fractures are the fundamental factors that determine the tight gas production. With these findings, this study is expected to guide the future exploration and development of tight gas with similar geological backgrounds.

## 1. Introduction

It is an inevitable trend in global petroleum exploration to transform from conventional to unconventional hydrocarbon resources (Zou *et al.* 2010, 2019; Yilmaz *et al.* 2016). Tight gas is an essential component of unconventional resources and will be the critical area in the global unconventional gas exploration (Law & Curtis, 2002; Higgs *et al.* 2007). Tight gas sandstones are usually characterized by low porosity, low permeability and natural fractures (Olson *et al.* 2009). Natural fractures play an essential role in controlling the accumulation of tight gas (Zeng & Liu, 2009; Zhang *et al.* 2018), and the enrichment of tight gas varies with the abundance of them (Schmoker, 1996; Ding *et al.* 2015). They can significantly improve the seepage capacity of the tight sandstone gas reservoir, providing an effective migration channel for hydrocarbon (Zeng, 2010; Lyu *et al.* 2017). The effectiveness of natural fractures is affected by structural diagenesis (Laubach *et al.* 2010).

According to the filling degree of natural fractures, three different kinds of natural factures can be classified: unfilled fractures, partially filled fractures and fully filled fractures, which can reflect the effectiveness of different fractures distinctly (Zeng *et al.* 2016; Zhao *et al.* 2017; Laubach *et al.* 2019). During the natural fractures opening or after the formation, they often undergo diagenesis; these geological processes could change the aperture and connectivity of fractures, which will have a complex impact on fluid flow process and dynamics (Laubach & Ward, 2006; Zhang *et al.* 2020). The natural mineralized fractures or fracture fillings provide valuable information for discriminating fracture sequence and genetic mechanism, and help to assess the evaluation of fracture opening, the origin of the circulating paleo-fluids and the openness of fluid system through time (Gasparrini *et al.* 2021).

The fact that permeability can be enhanced by natural fractures is vital in aquifers (Henriksen & Braathen, 2006; Maillot *et al.* 2016), waste repositories (Carey *et al.* 2015), hydrothermal systems (Sanderson *et al.* 1994) and petroleum reservoirs (Laubach, 2003; Gale *et al.* 2017; Wang, *et al.* 2020), including those in basement rocks (Cuong & Warren, 2009; Wang *et al.* 2019). The typical permeability of fracture-controlled reservoirs show tremendous heterogeneity and anisotropy in fluid flow (e.g. Halihan *et al.* 2000; Solano *et al.* 2011). Fracture network permeability is governed by many factors, including aperture and length distributions and connectivity, whether fractures are open or sealed, and the heterogeneous spatial arrangement of fractures (Wang *et al.* 2019). The fracture parallel to the current direction of maximum principal stress has a large aperture that can be regarded as the main seepage channel (Zeng & Li, 2009). Overall, fully filled fractures contribute little to reservoir productivity, while effective fractures are the main controlling factor for the single well productivity (Zeng *et al.* 2012*a*). It is therefore essential to research natural fractures for tight gas exploration and development.

In the Western Sichuan Foreland Basin of SW China, the proven natural gas reserves are approximately $3361.58 \times 10^8 \, \text{m}^3$ with an annual output of nearly $30 \times 10^8 \, \text{m}^3$ (Yang *et al.* 2012). As the Xujiahe Formation is rich in coal-bearing source rocks, continuous hydrocarbon accumulated in it (Zou *et al.* 2009). This formation therefore contains abundant natural gas resources within tight sand reservoirs and shows significant exploration potential (Zhang *et al.* 2016). For the study of tight gas reservoirs in the Xujiahe Formation, some predecessors paid much attention to diagenesis and pore characteristics (Liu *et al.* 2018*b*; Yue *et al.* 2018; Yu *et al.* 2019). Others emphasized the study of natural fractures of the Xujiahe Formation in the Xinchang gas field, including the basic types, genetic mechanism and formation period (Zhang, 2005; Ma *et al.* 2013; Deng *et al.* 2018; Yue *et al.* 2018), which has promoted the exploration and development of tight gas. Surprisingly, there is no related research on the effect of natural fractures on the accumulation and migration of tight gas, and the contribution of fractures to productivity also needs to be further summarized and discussed.

In this paper, we describe the fracture types, distribution characteristics, filling degree and apertures within the tight gas sandstones in the Upper Triassic Xujiahe Formation of the Xinchang gas field by utilizing drilling cores and image loggings. Through the relationships between cross-cutting fractures, we then summarize and synthesize the homogenization temperature measuring of fluid inclusion, carbon and oxygen isotopes, and quartz electron spin resonance (ESR). We also clarify the formation stage of natural fractures and the contribution of fractures in different stages of fluid to tight gas. At the same time, the influence of fracture strike and dip on fracture effectiveness is discussed. Finally, combined with regional geological data and hydrocarbon production, the effects of natural fractures on tight gas productivity are clarified. Research on the characteristics, formation, effectiveness and periods of the natural fractures in Xinchang area can improve the prediction accuracy of fracture distribution in the tight gas reservoirs and guide the in-depth exploration and development of tight gas.

## 2. Geological setting

The Sichuan Basin, located in the western part of the Yangtze Block, is a large composite gas-bearing and oil-bearing superimposed basin (Zheng *et al.* 2019). It connects Longmenshan Thrust Belt and Micangshan Tectonic Zone to the north,

Qian–Yu–Xiang–E fold belts to the south, Kang–Dian N–S zones to the west and Dabashan Tectonic Zone to the east (Fig. 1a). Since the beginning of the Late Triassic Epoch, the Sichuan Basin has experienced three periods of palaeo-tectonic movements during the Indosinian, Yanshanian and Himalaya movements. Its peripheral orogenic belts compress the basin from different directions in different stages, and the multi-stage and multi-directional structural systems are combined and modified in the basin (Liu *et al.* 2018*a*). The basin is divided into four tectonic units, namely: Western Sichuan Depression Belt, NE Sichuan Depression Belt, East Chongqing–SE Sichuan Depression Belt and Central Sichuan Uplift Belt (Fig. 1a). The Xinchang gas field is located in the Xinchang Structural Belt in the middle part of the Western Sichuan Depression, which is adjacent to Chengdu Sag to the south, Zitong Sag to the north and Zhixingchang– Longbaoliang structural belt to the SE, and intersects with the Longmenshan structural belt in the west (Fig. 1b).

The Palaeozoic, Mesozoic and Cenozoic sedimentary strata are present in the Western Sichuan Depression (Fig. 2). The Triassic strata includes the Upper Xujiahe Formation ($T_3x$), Maantang Formation ($T_3m$), Leikoupo Formation ($T_2l$), Lower Jialingjiang Formation ($T_1j$) and Feixianguan Formation ($T_1f$) (Jin *et al.* 2010). From bottom to top, the Xujiahe Formation is generally divided into five members (Zhao *et al.* 2011): $T_3x^1$, $T_3x^2$, $T_3x^3$, $T_3x^4$ and $T_3x^5$ (Fig. 2). Ma'antang–Xiaotangzi Formation ($T_3x^1$), $T_3x^3$ and $T_3x^5$ represent the critical source rock (Qin *et al.* 2018), which consists of dark mud shale of the shallow-sea shelf facies in the early stage, and grey carbon mud shales, sandstones and coal beds of delta limnetic facies in the middle and late–stages (Chen *et al.* 2012). The primary kerogen type of dark argillaceous source rocks is $II_2$–III kerogen. The maturity of source rocks is generally low mature to mature, with a vitrinite reflectance ($R_0$) of 0.8– 1.4% (Dai *et al.* 2007; Tao *et al.* 2014). $T_3x^2$ (burial depth > 4500 m; thickness 500–550 m) and $T_3x^4$ are the main reservoirs of the Xujiahe Formation. $T_3x^2$ was mainly deposited in the marine delta front, consisting mostly of distributary channels and mouth-bar sandstones (Luo *et al.* 2019). The lower part of $T_3x^2$ is mainly medium sandstone and fine sandstone with a small amount of mud shale; the middle part is mud shale, siltstone, fine sandstone and a few coal seams; the upper part is fine sandstone and medium sandstone with siltstone and mud shale. The $T_3x^2$ tight reservoir porosity is 1–4%, and the permeability is generally lower than 0.5 mD (Wang *et al.* 2020). In China, sandstone reservoirs with a measured porosity of < 10% and permeability < 1 mD at ambient laboratory conditions are categorized as tight sandstone reservoirs (Zou *et al.* 2013; Pang *et al.* 2019). On the whole, $T_3x^2$ in the Western Sichuan Depression is a typical tight reservoir.

## 3. Materials and methods

### 3.a. Characteristics of natural fractures

Fracture analysis was performed on the Xujiahe Formation interval of nine core wells of 906.62 m in the Xinchang gas field, and the fracture attributes were measured (filling degree, aperture, density and dip). Through image loggings processing and interpretation of 14 wells (4237.88 m), the types of natural fractures were determined, and the occurrence (strike and dip angle), aperture and density of the fractures were acquired (Ameen & Hailwood, 2008; Gong *et al.* 2019*a*). Finally, the influence of the natural fractures on the production of the single well was analysed by combining the trial production data of 14 wells (Table 1).
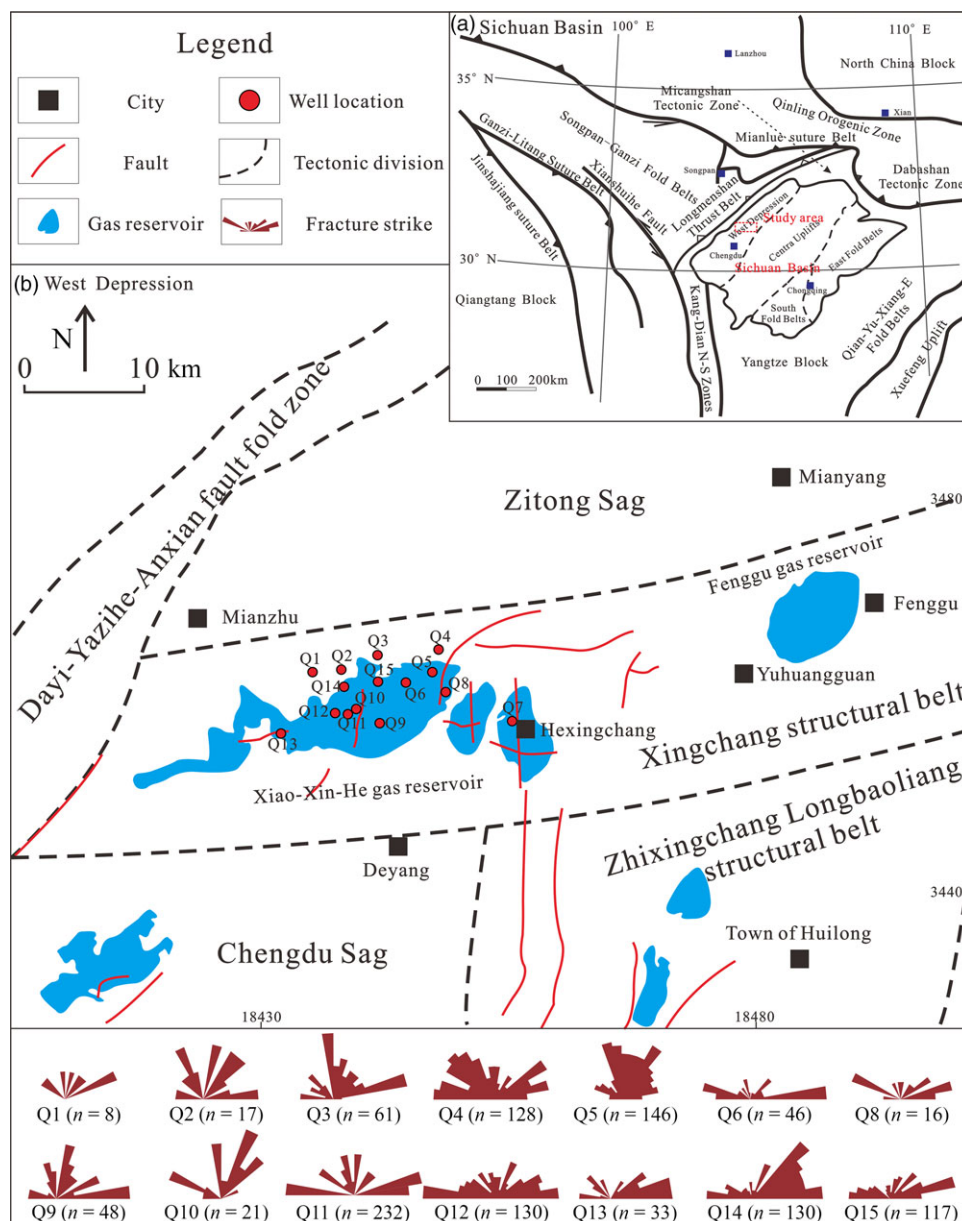
### 3.a.1. Fracture occurrence

To interpret the image loggings data, the natural fractures are first identified on the imaging map. A number of points are then selected on the fracture, extending the trajectory to fit the sine or cosine curves to calculate the inclinations and dip angles of the fracture (Zeng *et al.* 2010*b*).

### 3.a.2. Fracture aperture

When the measuring electrode of the image loggings tool is close to the natural fracture, the electrical resistance of the drilling fluid in the fracture will show an unusually low value; the electrode current of the instrument will then increase until the measuring electrode is far away from the fracture and unaffected by it. By using the three-dimensional finite element model, the response relationship between fracture width and resistance can be deduced. The formula for calculating fracture aperture is (Luthi & Souhaité, 1990; Ponziani *et al.* 2015):

$$W = CAR_m^b R_{xo}^{1-b}$$

$$A = \frac{1}{V_e} \int_{h_0}^{h_n} [I_b(h) - I_{bm}] dh$$

where $W$ is fracture aperture (mm); $b$ and $C$ are instrument parameters; $R_m$ is drilling fluid resistivity ($\Omega$m); $R_{xo}$ is the resistivity within the detection range of the instrument electrode ($\Omega$m); $A$ is the added value of the current caused by the fracture; $V_e$ is the potential difference between the measuring electrode and the upper return electrode (V); $I_b(h)$ is the current value of the electrode at a depth of $h$ ($\mu$A); $I_{bm}$ is the measured current value of the natural fracture ($\mu$A); $h_0$ is the initial depth at which the fracture affects the electrode measured values (m); and $h_n$ is the end depth of the influence of fractures on electrode measurements (m).
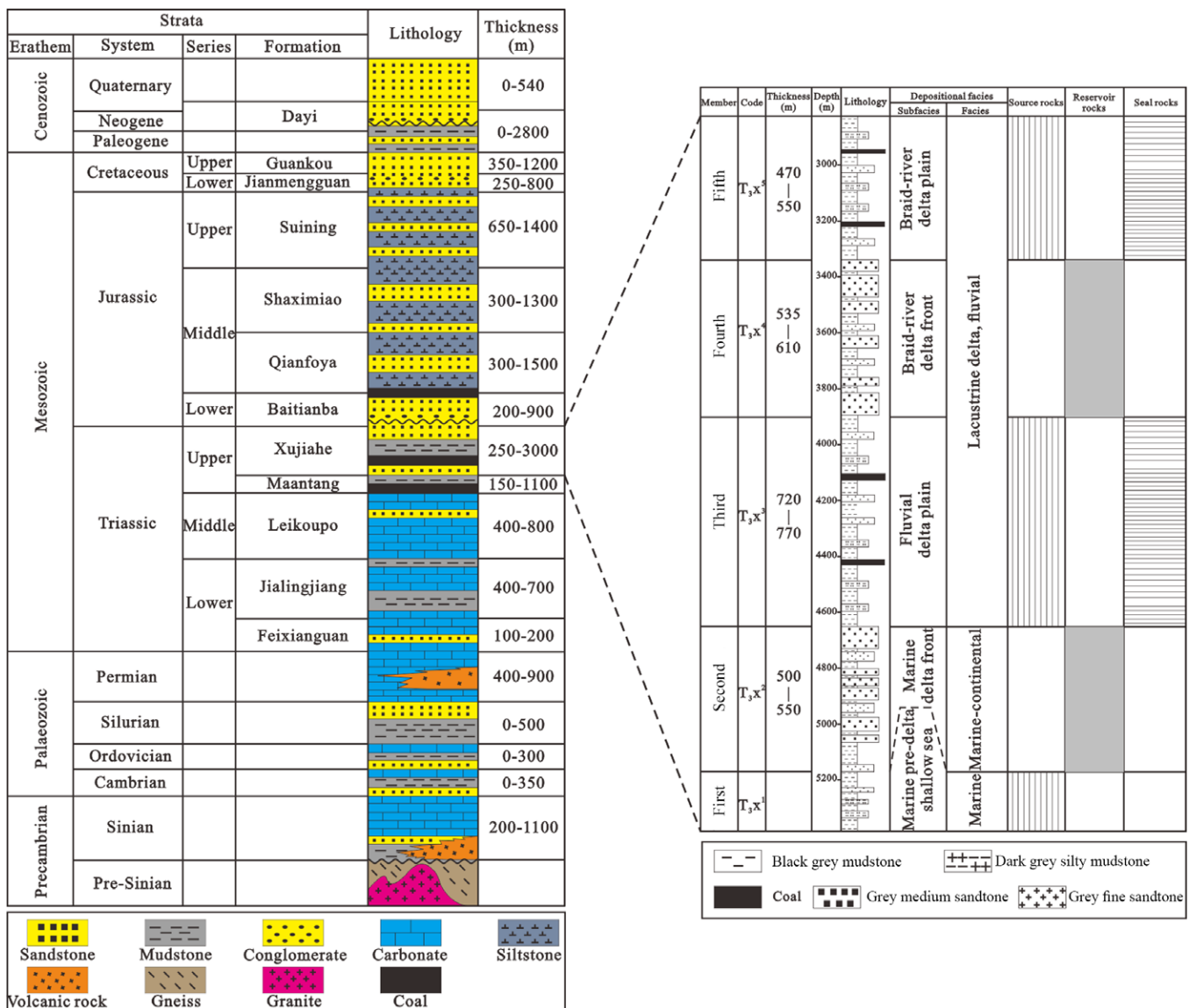
**Fig. 2.** (Colour online) The stratigraphic characteristics of Western Sichuan Depression and Upper Triassic Xujiahe Formation (modified from Li *et al.* 2014; Luo *et al.* 2019).

### 3.a.3. Fracture density

In image loggings, fracture density can be simply calculated as the number of fractures per unit length (Ameen *et al.* 2012; Lai *et al.* 2017):

$$F_d = \frac{1}{H}\sum_{i=1}^{n} L_i$$

where $F_d$ is the fracture density (m$^{-1}$); $H$ is the length of the evaluated well (m); and $L_i$ is the number of fractures in the evaluated wells.

### 3.b. Period of natural fractures

If cement is deposited while fractures are opening, the age of fractures can be determined by cement formation time (Laubach, 2003; Zeng *et al.* 2012b). The period of natural fractures can be obtained from the ESR and homogenization temperature measurement of fluid inclusions, which, combined with the burial and thermal

history, can help to constrain the fracture formation sequence (Zhang *et al.* 1995; Becker *et al.* 2010; Fall *et al.* 2015; Qiu *et al.* 2018; Wang *et al.* 2019).

## 4. Results

### 4.a. Natural fracture types and characteristics

#### 4.a.1. Core analysis

Natural fractures within the tight gas sandstones of the Upper Triassic T$_3$x$^2$ reservoir have been studied from cores and image loggings. These natural fractures are divided into tectonic fractures and diagenetic fractures from the perspective of their geologic origins.

As the primary type of natural fracture, the tectonic fracture is widely distributed in different kinds of lithology, with an obvious orientation and regular distribution. The surface of the fractures is smooth with the steps and slickensides as their typical features (Fig. 3a, b). Some of these fractures are filled with calcite or quartz. The density of tectonic fractures in siltstone is the highest, followed

**Table 1.** Summary of the research materials

| Well | Core (m) | Image logging (m) | Daily production | Initial production |
|------|----------|-------------------|------------------|--------------------|
| Q1 | | 506.34 | √ | √ |
| Q2 | | 458.39 | | √ |
| Q3 | 108.68 | 212.10 | | |
| Q4 | 30.51 | 296.72 | | |
| Q5 | 284.40 | 439.85 | √ | √ |
| Q6 | 5.62 | 247.25 | | √ |
| Q7 | 70.21 | | | |
| Q8 | | 76.38 | | |
| Q9 | | 165.23 | √ | √ |
| Q10 | | 393.06 | | √ |
| Q11 | 9.00 | 54.90 | √ | √ |
| Q12 | | 326.86 | | √ |
| Q13 | | 221.84 | | |
| Q14 | 145.70 | 462.78 | | |
| Q15 | | 376.18 | √ | √ |
| Q16 | 36.98 | | | |
| Q17 | 215.52 | | | |
| Total | 906.62 | 4237.88 | 5 | 9 |

by those in fine sandstones and medium sand; the fracture density of gritstone is the lowest (Fig. 4). With the increase of sandstone particle diameter, the density of natural fractures decreases. The tectonic fracture can be subdivided into five types according to dip angle: nearly vertical fractures (> 80°), high-angle fractures (60–80°), middle-angle fractures (30–60°), low-angle fractures (10–30°) and nearly horizontal fractures (< 10°) (Zeng *et al.* 2010*b*). The nearly horizontal fractures are mainly developed in medium sandstone and gritstone, and intersected with the plane at a small angle (Fig. 3c). They usually have equal spacing of 3–5 cm.

The main type of diagenetic fracture is bedding fractures, which are generally developed along the plane in interruption characteristics, that is, bending, wedge-out, combining or branching out along the plane (Fig. 3d). The bedding fractures are widely distributed and developed in the study area, but their extending length has not yet been identified. The stylolite is usually in a serrated shape with insoluble minerals, and the organic matter remains abundant (Fig. 3e).

### 4.a.2. Image loggings analysis
Natural fractures typically appear as a sine or cosine curve pattern in the image loggings; the colour is generally different from the surrounding formations. Their width and amplitude are controlled by fracture aperture and dip angle, respectively (Fig. 5). The results of image loggings interpretation show four dominant assemblages of natural fracture in the $T_3x^2$: E–W, NE–SW, N–S and NW–SE strike (Figs 1, 6).

### 4.b. Cross-cutting relationships
By analysing the cross-cutting relationships of different genetic fractures in cores and the characteristics of their fracture fillings,

we can effectively reconstruct the natural fracture sequence (Felici *et al.* 2016; Kanjanapayont *et al.* 2016). The filling degree also can illustrate the formation timing of different fractures, and the filling degree of different genetic fractures formed in the same period is similar (Li *et al.* 2021). The filling minerals in the fractures include calcite, quartz, carbonaceous clay and asphaltene (Fig. 7). Quartz and calcite are filled in tectonic fractures, and carbonaceous clay is usually filled in bedding fractures. Based on the cross-cutting relationships of natural fractures, three phenomena can be clearly observed. (i) Three types of calcite fillings cut and restricted each other based on the degree of crystallization and filling (Fig. 7a–c), indicating that the fracture experienced three stages of calcite filling. (ii) Some bedding fractures are filled with carbonaceous clay while others are not, and there are tectonic fractures filled with asphaltene and carbonaceous clay that restrict the bedding fractures without filling (Fig. 7d). The second phenomenon indicates that bedding fractures experienced one period of carbonaceous clay filling event and one period without any filling event, and the carbonaceous clay filling preceded the no-filling. (iii) Tectonic fractures are filled with calcite, quartz and asphaltene (Fig. 7e), and the asphaltene fillings are on the surface of quartz and calcite, indicating that the quartz and calcite filling event was earlier than the asphaltene filling event. Based on the above analysis, the four filling stages of natural fractures can be initially determined. Firstly, the tectonic fractures were filled with calcite and quartz. Secondly, the bedding fractures were filled by carbonaceous clay. Thirdly, the tectonic fractures were filled with calcite and asphaltene. Finally, the tectonic fractures were filled with calcite.

## 5. Discussion

The tectonic fractures are related to tectonic processes (Aguilera, 1998; Lyu *et al.* 2017). Diagenetic fractures result from volumetric reductions caused by diagenetic changes within rocks (Aguilera, 1998; Shi *et al.* 2020). Bedding fractures are constrained and controlled by depositional bedding (Petrie *et al.* 2014), indicating that they were formed during the diagenetic processes of the reservoir (Gong *et al.* 2019*b*). The formation of stylolite is closely related to the dissolution of rocks driven by compressive stress (Brouste *et al.* 2007). These fractures are related to diagenesis, rather than the result of tectonic events (Zeng & Li, 2009; Lyu *et al.* 2017; Zhang *et al.* 2020; Liu *et al.* 2020).

### 5.a. Fracture sequence

#### 5.a.1. Homogenization temperature of fluid inclusions
Cements within fractures are precipitates of the fluid during fracture opening (Laubach, 1988; Fall *et al.* 2015; English & Laubach, 2017); they therefore provide important clues to fluid composition, pressure and temperature conditions in retracing the fracture-opening history (Hooker *et al.* 2009; Lander & Laubach, 2014). Fluid inclusions within fracture cements are micron-scale volumes of the fluid entrapped during the precipitation of minerals (Watson & Brenan, 1987; Baron *et al.* 2008). The relative timing of the fluid inclusion assemblages (FIAs) is constrained by textural mapping of fracture-growth cement zones, allowing us to place the fractures in their orogenic context by correlation with independently derived burial history (Becker *et al.* 2010; Fall *et al.* 2012; Liu *et al.* 2020). Becker *et al.* (2010) found that fluid inclusions within quartz are common in sandstones and preferable for the reconstruction of fluid-inclusion palaeotemperatures compared
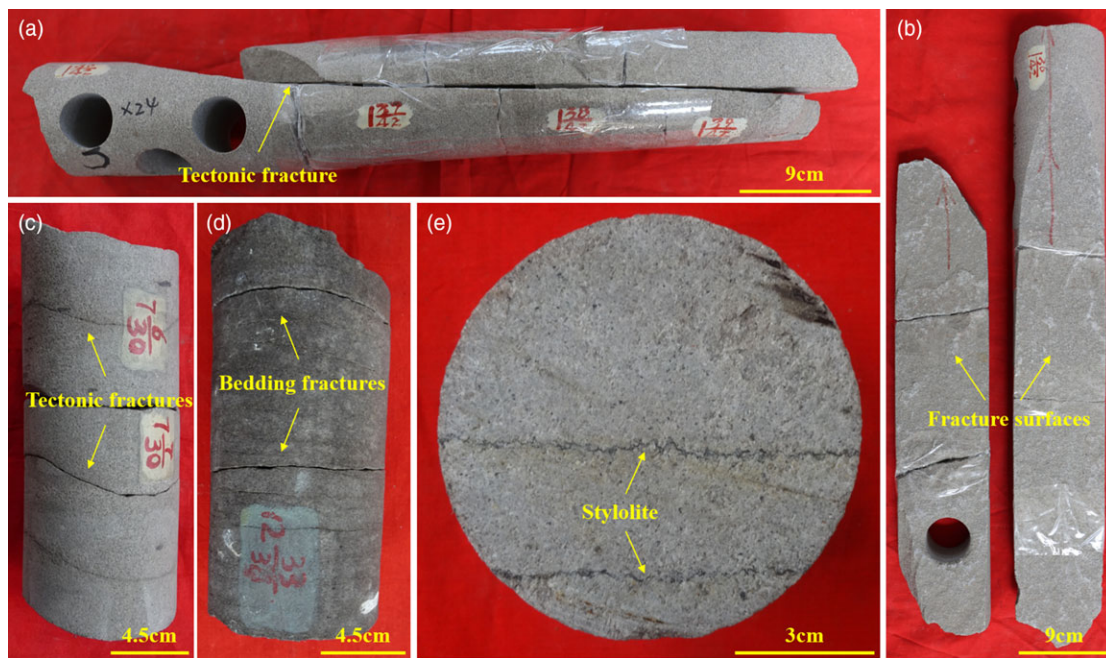
**Fig. 3.** (Colour online) Natural fractures of the cores. (a) High-angle tectonic fracture from well Q6, at a depth of 4733.95 m; (b) The joint surface of high-angle tectonic fractures in (a); (c) low-angle tectonic fracture from well Q3, at a depth of 4918.55 m; (d) bedding fractures from well Q5, at a depth of 5026.95 m; (e) stylolite from well Q5, at a depth of 4931.46 m.
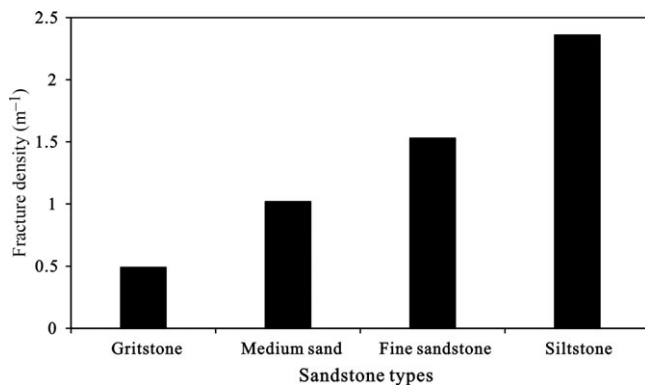


**Fig. 4.** The relationship between sandstone types and tectonic fracture density; the diameters of gritstone, medium sandstone, fine sandstone and siltstone are 0.5–2.0, 0.25–0.50, 0.10–0.25 and 0.01–0.10 mm, respectively.

with fluid inclusions in carbonate minerals, which may experience volumetric re-equilibration due to the relative low hardness of minerals (Pecher, 1981; Liu *et al.* 2013). An improved ability to accurately map crack-seal textures in carbonate cements would make it possible to describe the temperature sequences during fracture opening in carbonates (Ukar & Laubach, 2016), following a similar method to that used for quartz-filled fractures in sandstones (Becker *et al.* 2010; Fall *et al.* 2015). Stretched or leaked inclusions will yield homogenization temperatures ($T_h$) greater than undeformed inclusions (Gao *et al.* 2017). To avoid the anomalous homogenization temperatures resulting from volumetric re-equilibration, heating runs were conducted before freezing runs to reduce the possibility of inclusion stretching by freezing. By restricting measurements to inclusions within the same field of view, any sudden changes in liquid and/or vapour ratios due to inclusion deformation could be observed and removed from consideration (Liang *et al.* 2019). Where possible, only the smallest

inclusions and/or those with rounded and smooth walls were measured, as they give the most reliable $T_h$ values (Ulrich & Bodnar, 1988; Osborne & Haszeldine, 1993). However, if the fluid inclusions in the fractures are affected by hydrothermal action, their measured temperatures may be significantly higher than the maximum temperatures of burial history and thermal evolution, and the periods of these fractures become difficult to determine. The homogenization temperature of tectonic fracture ranges from 80 to 240°C, and the peak temperatures are distributed over 80–120, 160–200 and 200–240°C, respectively (Fig. 8a). The homogenization temperature of bedding fractures varies from 120 to 240°C, and the peak temperatures are within the ranges 120–160 and 200–240°C (Fig. 8b). The peak temperatures of fluid inclusions in netted fractures are within the ranges 160–200 and 200–240°C (Fig. 8c).

*5.a.2. Electron spin resonance dating*
ESR refers to the resonance absorption effect caused by the magnetic moment of unpaired electron spin (Ren *et al.* 2016). When the magnetic moment of the electron spin in the stationary magnetic field is affected by a radio-frequency (RF) electromagnetic field, the electron will resonate with the RF electromagnetic field and transit from the low-energy product to the high-energy product (Hennig & Grün, 1983). The ESR dating of fault/fracture movements assume that the ESR signals in rock-related features are reset during faulting/fracturing as a result of the heat generated by friction and/or intense deformation (Tsakalos *et al.* 2018). This method has been widely used in seismic geology, engineering geology and geological sciences (Huang, 1994; Qiu *et al.* 2018; Voinchet *et al.* 2019). The age of one substance, such as quartz and calcite, can be determined by measuring the dosage of radiation after their formation (Ren *et al.* 2016). Under the bombardment of the natural rays generated from the fracture wall, the earlier that the authigenic minerals (quartz or calcite veins) in the fractures are formed,
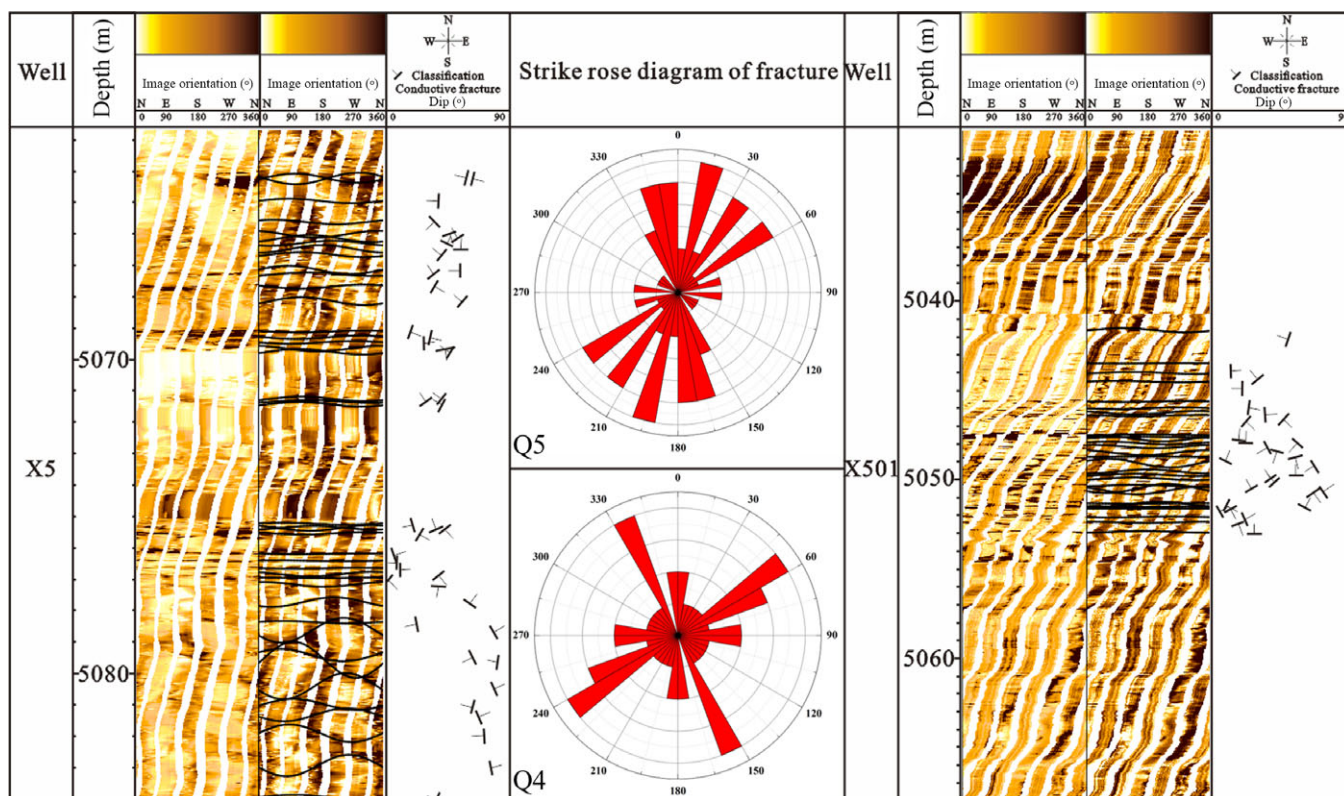
**Fig. 5.** (Colour online) Fractures detected by image loggings in wells Q5 and Q4. All fractures in the image loggings are open.
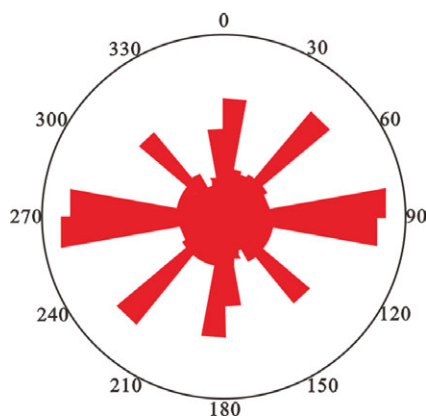


**Fig. 6.** (Colour online) Rose diagram of the fracture strikes in the $T_3x^2$ tight gas sandstones in the Western Sichuan Basin. The data were obtained from image loggings ($n = 1133$).

the higher the paramagnetic centre concentration (Zhang *et al.* 1995). ESR can therefore directly determine the age of the secondary minerals in the fracture, and approximately represent the formation time of the natural fracture. The relative error of an ESR age is related to the experimental conditions. The error can be introduced by statistical errors, natural radioactive decay of the element's uranium and thorium, the standard applied and the instrumental error (Liang & Gao, 1999). The total error is less than 10% of the absolute age (Peng *et al.* 1993). Different from carbon and oxygen isotopes and fluid inclusion thermometry, ESR dating can directly obtain the approximate age of natural fractures. It is not necessary to determine the formation time of natural fractures

by matching the temperature obtained directly or indirectly with the thermal history. The formation time of quartz fillings in the fracture was 217 and 219 Ma according to quartz ESR dating, and the fracture formed during the late Indosinian tectonic movement (Table 2).

According to the cross-cutting relationship of minerals in fractures, their fluid-inclusion analysis, quartz ESR dating and burial history, we determine three fracture-filling events, showing that tectonic fractures were mainly formed during three tectonic periods. The first event was at the end of the Triassic Period, with fluid-inclusion homogenization temperatures ranging from 80 to 120°C and quartz fillings of age 217–219 Ma (Fig. 9 and Table 2). The second event occurred during the Cretaceous Period, with fluid-inclusion homogenization temperatures ranging from 160 to 200°C (Fig. 9). The third event occurred during the Palaeogene Period, with fluid-inclusion homogenization temperatures ranging from 200 to 240°C (Fig. 9). Two stages of bedding fractures were formed during the middle and late Indosinian and late Yanshanian orogenic periods (Fig. 9).

## 5.b. Source of calcite fillings in the fracture

Carbon isotope ratios can be used to reflect the sources of carbon, including bacterial sulphate reduction, fermentation, dissolution of carbonate minerals, methane oxidation, methane production and organic matter decarboxylation (Morad *et al.* 1990; Fayek *et al.* 2001). The oxygen isotope ratio of minerals is controlled mainly by the variation range of temperature (burial depth), the degree of fractionation between fluid and minerals, and the fluid source (Chowdhury & Noble, 1996). The carbon and oxygen isotopic compositions of fracture fillings also record the temperature and
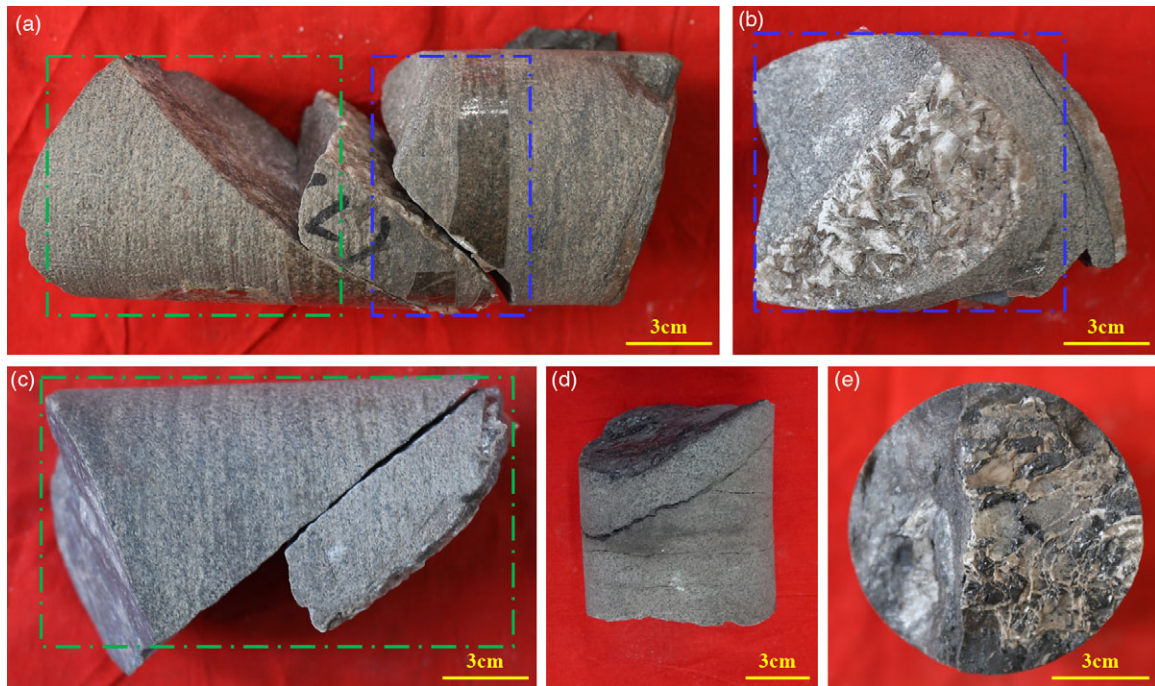
**Fig. 7.** (Colour online) Fracture cross-cutting and abutting relationships from cores. (a–c) Three types of calcite fillings cut and restricted each other based on the degree of crystallization and filling from well Q4, at a depth of 5252.29 m. (d) Carbonaceous clay fills some bedding fractures, but not all. Some tectonic fractures are filled with asphaltene and carbonaceous clay from well Q5 at a depth of 4967.56 m. (e) Tectonic fractures are filled with calcite, quartz and asphaltene in well Q4, at a depth of 5252.87 m.
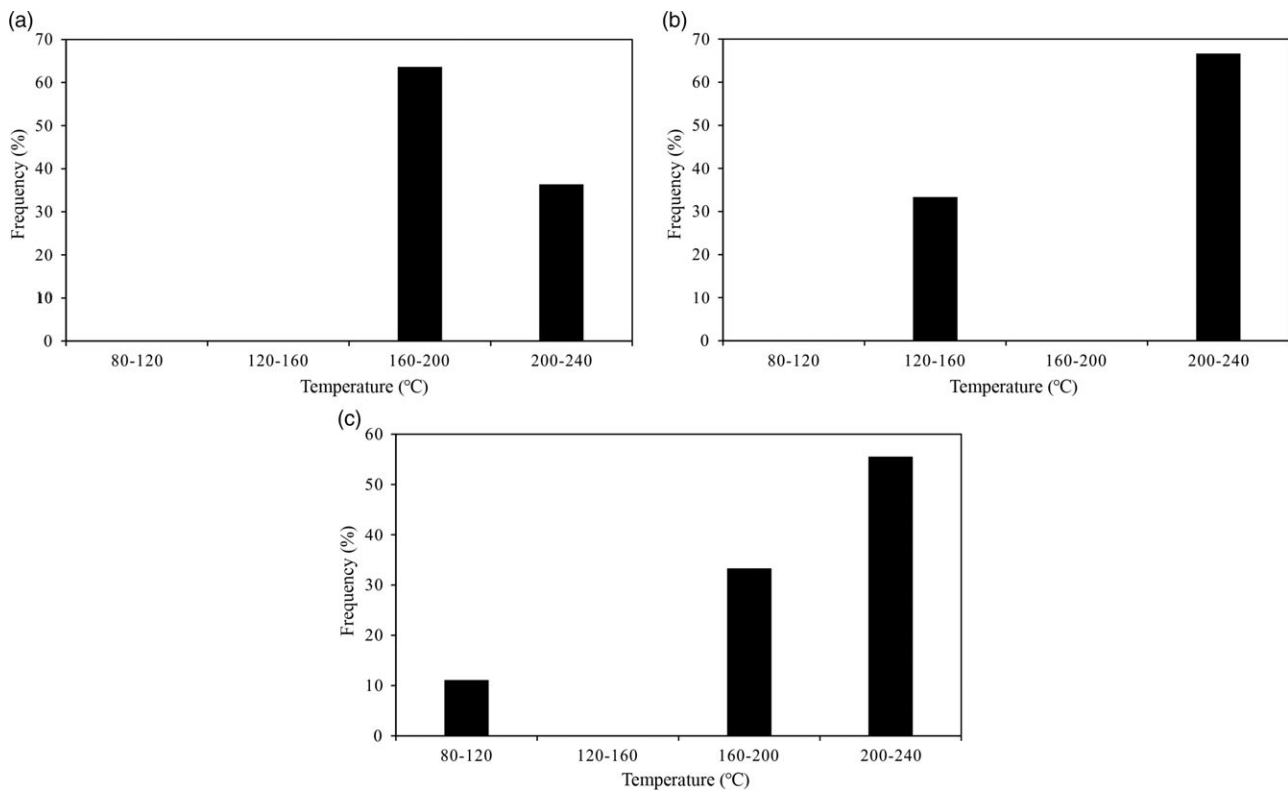


**Fig. 8.** Frequency histogram of homogenization temperature from inclusions in fracture calcite fillings in $T_3x^2$: (a) in the tectonic fracture ($n = 11$); (b) in the bedding fracture ($n = 6$); and (c) in the netted fracture ($n = 9$). The test data were obtained from Yang *et al*. (2012) and Deng *et al*. (2013).

**Table 2.** Results of quartz electron spin responance dating in the $T_3x^2$ sandstone of Xinchang area, Western Sichuan Basin

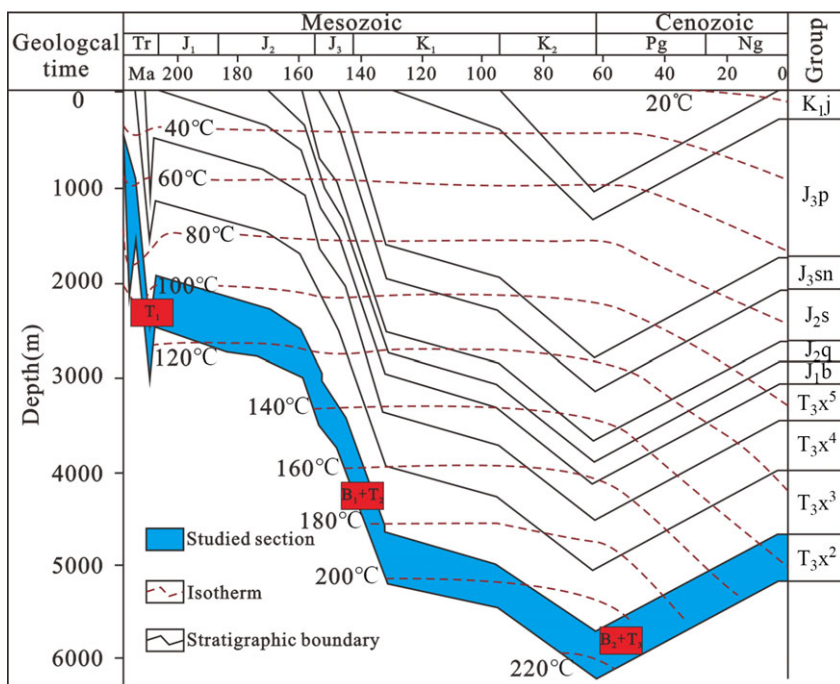| Well | Depth (m) | Minerals | Age (×10⁸ a) | Tectonic deformation generation | Reference |
|------|-----------|----------|--------------|---------------------------------|-----------|
| CH138 | 4596.81 | Quartz | 2.19 | Late Indosinian | Zhang (2005) |
| CX127 | 4578.23 | Quartz | 2.17 | Late Indosinian | |



**Fig. 9.** (Colour online) Burial history, thermal history and the temperature of calcite fillings in the fractures in the Triassic Xujiahe Formation (Leng *et al.* 2011). Tr – Triassic; J – Jurassic; K – Cretaceous; Pg – Palaeogene; Ng – Neogene. $T_1$ – first stage of tectonic fracture; $T_2$ – second stage of tectonic fracture; $T_3$ – third stage of tectonic fracture; $B_1$ – first stage of bedding fracture; $B_2$ – second stage of bedding fracture.

salinity information about the fracturing fluids (Spero *et al.* 1997; Liu *et al.* 2020; Zhang *et al.* 2020). By comparing with the host rock and the target layer, we can infer the fluid origin (Hooker *et al.* 2015; Zhang *et al.* 2017). In the interpretation of carbon isotope values of carbonate cements, the biggest challenge is that there may be two or more sources of carbon, and the later diagenetic recrystallization will interfere with the interpretation of the source of dissolved carbon (Morad *et al.* 1990; Liu *et al.* 2014). The timing of three stages agrees with the inferences from carbon- and oxygen-stable isotope analysis of calcite fillings in tectonic fractures (Ma *et al.* 2013). It is possible for us to analyse the source of calcite fillings in tectonic fractures from different stages. The $\delta^{13}C$ values of calcite fillings in fractures range from –9.061 to 1.853‰, with an average value of –0.951‰; the $\delta^{18}O$ value varies from –10.371‰ to –17.575‰, with an average value of –15.613‰ (Table 3). The $\delta^{13}C$ values of calcite in the matrix range from –1.33‰ to 1.70‰ with an average value of 0.09‰, and the $\delta^{18}O$ values varies from –16.65‰ to –10.88‰, with an average of –14.07‰ (Table 3).

The carbonate cements of the Xujiahe Formation sandstones can be divided into two generations of early and late carbonate cement, and the sandstone was dominated by late calcite (Luo *et al.* 2019). The $\delta^{13}C$ values of early calcite cement in the residual primary pores is –0.33‰. The carbon source of the early calcite cement in the pores is closely related to the internal carbonate rock fragments consisting of inorganic carbon, whose $\delta^{13}C$ values can increase up to 3‰ (Friedman & O'Neil, 1977). Because of the Longmenshan uplift during the Late Triassic Epoch, the Palaeozoic marine carbonate strata in the west of the Sichuan

Basin had experienced intense erosion, and abundant carbonate fragments were supplied to the Xujiahe sediments by river transportation (Xu *et al.* 2015; Liu *et al.* 2019). Given that the average value of $\delta^{13}C$ in carbonate fragments is +1.93‰ (Liu *et al.* 2014), the observation indicates that the carbonate rock fragments are providing another carbon source for the carbonate cements in the Xujiahe Formation (Li *et al.* 2019). However, there was not enough acid for the dissolution of internal carbonate rock fragments at the early diagenetic stage. The early calcite cement in the pores therefore precipitated from pore fluids containing $Ca^{2+}$ and $CO_3^{2-}$ came from the original formation water in sandstone and adjacent mudstone, which were mainly related to weathering or the dissolution of carbonate rock fragments in the provenance or transport process, and were rarely related to the organic carbon/acid. The fact that the mixed carbon source was mainly composed of carbon rock fragments and the original formation water meant that the negative $^{13}C$ value of calcite cement in the residual primary pores was < 3‰. The $\delta^{13}C$ values of late calcite cement in the secondary pores are –1.25‰ and +1.70‰ (Fig. 10). The source rock in the lower sub-member of $T_3x^2$ exists under methanogenic conditions (Luo, 2015). The organic acid in $T_3x^1$ and lower sub-member of $T_3x^2$, which migrated into the sandstone reservoir of the marine-source rocks, provided the carbon source for carbonate cement in the reservoir matrix pores (Liu *et al.* 2014; Luo, 2015). The isotope data reveal the mixing between organic-derived carbon and inorganic-derived carbonate cements, and the inorganic carbon is dominant, so the $\delta^{13}C$ values of late calcite cements are relatively heavy. The $Ca^{2+}$ may come from

**Table 3.** Types and isotopic features of calcite cements and fillings in the $T_3x^2$ sandstone of Xinchang area, Western Sichuan Basin

| Well | Depth (m) | Types of occurrence (dip) | $\delta^{13}C_{PDB}$ (‰) | $\delta^{18}O_{PDB}$ (‰) | Tectonic deformation generation |
|------|-----------|---------------------------|--------------------------|--------------------------|---------------------------------|
| Ma *et al.* (2013) | | | | | |
| XC6 | 5001.15 | Fracture filling (L) | −8.412 | −11.928 | Late Indosinian |
| X5 | 4933 | Fracture filling (NV) | −9.061 | −10.371 | Late Indosinian |
| CX565 | 5051.88 | Fracture filling (NV) | −1.194 | −13.424 | Yanshanian |
| CX565 | 5058.66 | Fracture filling (NV) | −3.017 | −14.104 | Yanshanian |
| CX565 | 5048.26 | Fracture filling | 0.561 | −17.575 | Himalayan |
| X5 | 4737.07 | Fracture filling (NV) | 1.359 | −16.868 | Himalayan |
| X501 | 5269.7 | Fracture filling | −0.827 | −16.167 | Himalayan |
| CX565 | 5050.88 | Fracture filling (L) | 0.387 | −17.33 | Himalayan |
| X501 | 5251.35 | Fracture filling | −0.285 | −15.851 | Himalayan |
| CX565 | 4905.12 | Fracture filling (H) | 1.653 | −17.292 | Himalayan |
| CX565 | 5053.9 | Fracture filling (M) | 1.853 | −17.564 | Himalayan |
| CX565 | 5060.83 | Fracture filling (NV) | 0.408 | −15.596 | Himalayan |
| XC6 | 5012.35 | Fracture filling (L) | 1.306 | −17.173 | Himalayan |
| CX565 | 5062.5 | Fracture filling (NV) | 0.476 | −16.771 | Himalayan |
| CX565 | 5049.38 | Fracture filling (NV) | 0.529 | −16.185 | Himalayan |
| Luo *et al.* (2019) | | | | | |
| XC12 | 4819.45 | Rpp and Sp | −0.06 | −16.65 | – |
| GM2 | 4992.3 | Rpp and Sp | −1.33 | −16.09 | – |
| GM4 | 5114.97 | Rpp and Sp | 0.05 | −12.64 | – |
| XC8 | 5175.37 | Rpp and Sp | −0.11 | −12.47 | – |
| XC7 | 5287.98 | Rpp and Sp | 0.99 | −12.98 | – |
| XC7 | 5291.33 | Rpp and Sp | 1.15 | −13.45 | – |
| X11 | 4755.72 | Rpp and Sp | 0.05 | −12.56 | – |
| CG561 | 4997.72 | Rpp and Sp | 1.70 | −16.36 | – |
| X11 | 5070.01 | Rpp and Sp | −1.25 | −16.64 | – |
| X11 | 5075.64 | Rpp and Sp | −0.33 | −10.88 | – |

NV – nearly vertical fractures; H – high-angle fractures; M – middle-angle fractures; L – low-angle fractures; Rpp – residual primary pore; Sp – secondary pore.
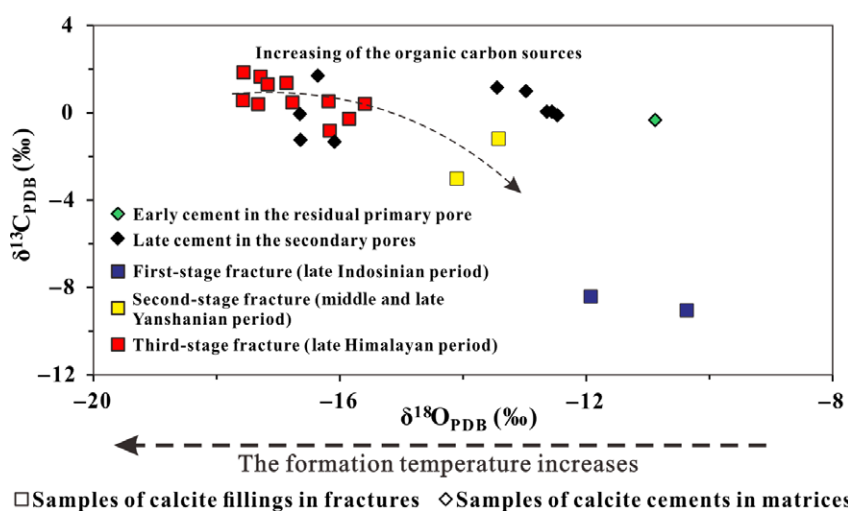


**Fig. 10.** (Colour online) Carbon and oxygen isotope results. The data describing the calcite fillings in tectonic fractures are from Ma *et al.* (2013); calcite data in the matrix are from Luo *et al.* (2019).

the late dissolution of feldspar and rock fragments and from the transformation of clay minerals during the burial progress (Xi *et al.* 2015).

The $\delta^{13}C$ values of calcite fillings in the first stage of fractures are –8.412‰ and –9.061‰ (Fig. 10). The $\delta^{13}C$ value of the carbonate cement filling is approximately –7‰, which means that the source of $\delta^{13}C$ was modified by the meteoric water (Mack *et al.* 1991; Spötl & Wright, 1992). The reservoir in the formation period was shallow in depth, and the meteoric water flew through the fracture to the underground to participate in the formation of the calcite filling. The $\delta^{13}C$ values of calcite fillings in the second stage of fractures are –3.017‰ and –1.194‰ (Fig. 10), indicating that these carbonate fillings are mainly formed under methanogenic conditions or during oxidation of organic carbon (Irwin *et al.* 1977; Wei *et al.* 2015). The $CO_2$ generated from thermal decarboxylation of organic matter or hydrocarbon oxidation by sulphate or manganese reduction is depleted in $\delta^{13}C$ (Irwin *et al.* 1977; Wu *et al.* 2017). The late calcites cement in the secondary pores and that in the second stage of fractures have similar carbon values, and the former is slightly heavier than the latter. The methanogenesis can leave behind a pool of enriched carbon in the secondary pores, and the light components were migrated through the fractures and participated in the formation of calcite fillings in the fractures. This can be used to explain the minor difference between the two carbon values. Carbon sources of carbonate fillings could therefore have come from the organic acids that flowed into sandstone from the source rock (Liu *et al.* 2014). The $\delta^{13}C$ values of calcite fillings in the third fracture fillings are between –0.827 and +1.853‰. Further, the late calcites cement in the secondary pores and the third stage of fractures have similar carbon values. In this period, the $T_3x^2$ reservoir has transformed from a moderately open system to a closed system (Luo *et al.* 2019). These fracture-filling carbonates have identical carbon to the sediment of the host rock, and therefore probably formed by closed-system dissolution-reprecipitation of host-rock carbonates. Compared with the second-stage tectonic fracture fillings, the contribution of organic carbon in the third stage fracture fillings is lower and the $\delta^{13}C$ value is increased, which may be related to the reduction in hydrocarbon generation.

## 5.c. Relationship between fracture evaluation and tight gas accumulation and migration

The tight gas accumulation periods covered $T_3x^5$ – Early Jurassic (the first gas accumulation phase), Middle Jurassic – Early Cretaceous (the second gas accumulation phase) and Himalayan (the third gas accumulation phase). Among them, the second gas accumulation stage spanned the longest period (Liu *et al.* 2009) (Fig. 11). According to the burial history and thermal history analysis, the gas molecular events of tectonic fractures occurred Early Cretaceous and Eocene time. The oil and gas molecular events of bedding fractures occurred during the Late Jurassic and Late Cretaceous periods.

When the natural fracture was completely filled with minerals, most of the fracture storage space and percolation path were lost (de Graaf *et al.* 2017). The first-stage tectonic fractures were formed earlier than calcite and quartz cementation, so they experienced longer cementation and were prone to be filled with minerals and present poor effectiveness (Zeng *et al.* 2012a). This tectonic fracture exhibited poor effectiveness for tight gas charging, and can only provide a small amount of reservoir space and seepage channel in the later stage. Although compaction and

cementation significantly reduced the porosity and permeability of the reservoir (Lézin *et al.* 2009; Lavenu *et al.* 2014), they improved the overall brittleness of the reservoir (Zeng *et al.* 2016; Zhang *et al.* 2020). A better brittle condition of the reservoir provided favourable conditions for forming the second-period tectonic fractures and the second stage of cementation was at the initial stage of diagenesis, so the cementation was relatively weak. The development strength and the effectiveness of the tectonic fractures formed in this period were therefore superior to that of the first stage. The formation time of the second-stage tectonic fracture was consistent with the main-reservoir-forming time. The fracture occurred after reservoir densification, and the tectonic fracture greatly improved the low porosity and permeability of the reservoir. Hydrocarbon was primarily generated and expelled during the main tight gas accumulation period, and the second-stage tectonic fractures provided the seepage channels and important reservoir spaces for the vertical migration of natural gas in the tight sandstone. The main diagenesis in $T_3x^2$ was almost complete, and the cementation was at its end stage (Fig. 11). At this time, the reservoir was the tightest, and the rock brittleness was the most favourable, so the development and effectiveness of the third-stage tectonic fracture were the best among all the three stages. In this period, the tectonic fractures were consistent with the accumulation time of tight gas in the third gas accumulation phase and greatly improved the permeability of the reservoir, adjusted and reconstructed the primarily sealed gas reservoir, and restored the seepage capacity of the tight reservoir.

The beddings formed in the early deposition period contributed to the reservoir as the primary pores and had better reservoir space and seepage capacity. Here, the bedding with seepage capacity is referred to as the primary bedding fracture. During the middle and late Indosinian period, $T_3x^2$ sediments within reservoirs were compacted into rocks and transformed by diagenesis. The bedding fractures were compacted vertically, resulting in a reduced or even closed aperture. The compaction was therefore the main diagenetic type that weakened the migration capacity of bedding fractures in the early stage of formation. However, in the high-quality reservoirs with low matrix and muddy content and with strong compaction resistance, the bedding fractures maintained seepage ability (Fig. 12a). The primary bedding fractures could be used as transverse short-distance migration channels for tight gas accumulation during the first and second tight gas charging (Fig. 12b). It was found that the homogenization temperature fluid inclusions in the primary bedding fractures (120−160°C) were lower than that in the second-stage tectonic fractures (160–200°C). This could indicate that the tight gas reservoir initially underwent short-distance transverse migration. When it encountered fractures with middle and high angles, it then began to migrate vertically. The primary bedding fractures improved the physical property of the reservoir and accelerated the migration of tight gas. During middle Yanshanian time the reservoir experienced the main mechanical compaction, and the bedding fractures had the least contribution to the gas migration. In geological history the stratum was uplifted, changing the aperture of the bedding fractures (Gale *et al.* 2017). The tectonic uplift mainly reduced the minimum principal stress, so that the Mohr Circle of stress could be increased to intersect the rupture envelopes (Zeng *et al.* 2010a) and the bedding fractures could reopen. At the end of the Early Cretaceous Epoch, the stratum was significantly uplifted (Fig. 9). The pressure unloading within the early closed bedding fractures could have led to the reopening of beddings and bedding fractures. The primary bedding fractures and the second-stage tectonic fractures combined
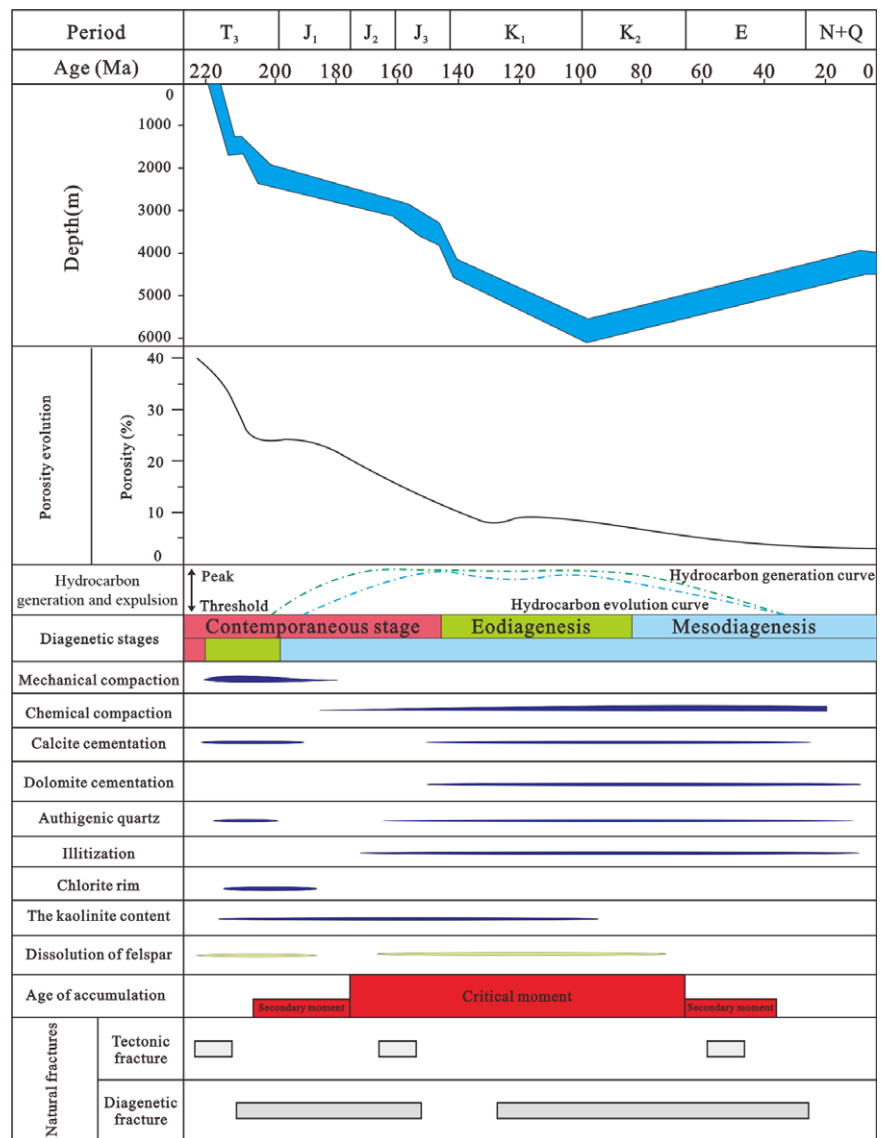
**Fig. 11.** (Colour online) Petroleum system event and fracture formation time of the Triassic Xujiahe Formation. Data describing pore evolution and diagenesis of the reservoir are from Liu *et al*. (2018*b*) and Yu *et al*. (2019); data describing efficiency of hydrocarbon expulsion and petroleum system event are from Guo *et al*. (2012). T – Triassic; J – Jurassic; K – Cretaceous; Pg – Palaeogene; Ng – Neogene; Q – Quaternary.
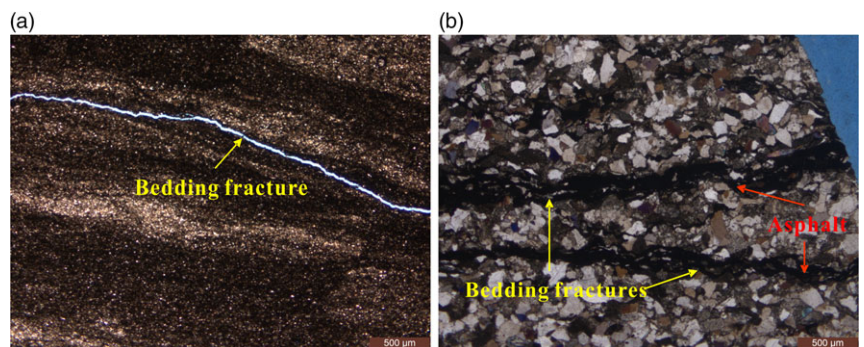


**Fig. 12.** (Colour online) Evidence that bedding fractures maintain the seepage ability and enable the hydrocarbon to migrate. Bedding fracture in (a) well Q11, depth 4718.19 m and (b) well Q5, depth 6062.40 m. Cross-polarized light images.

to form the early fracture network system. In contrast, the late ruptured bedding fractures and the third-stage tectonic fractures together constituted the late fracture network system. The peak temperature distribution range of fluid inclusions of fillings in netted fractures covers the temperature range of fluid inclusions in bedding fractures and tectonic fractures, which can be used as strong evidence for the formation of multi-stage fracture networks.

### 5.d. Factors affecting the effectiveness of natural fractures

The maximum principal stress orientation of $T_3x^2$ in the Xinchang gas field is close to an E–W trend (Cao, 2005); so the average aperture value (0.126 mm) of E–W-aligned fractures is therefore greater than that of NW-aligned (0.094 mm) and NE-aligned (0.087 mm) fractures (Fig. 13a). The N–S fractures are
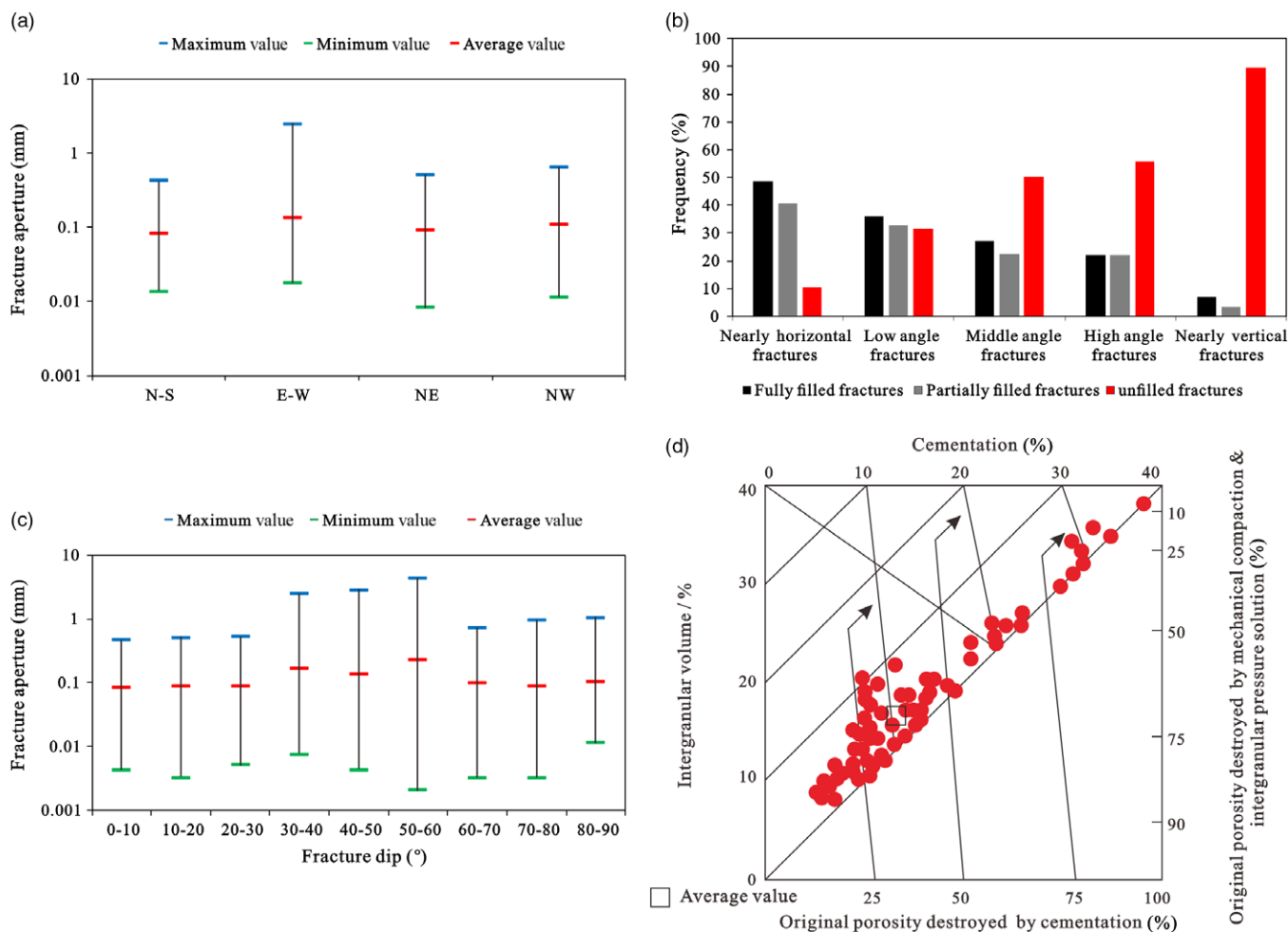
**Fig. 13.** (Colour online) (a) The relationship between fracture strike and fracture aperture. (b) The distribution of filling degree in different fracture dips. (c) The relationship between fracture dip and fracture aperture. (d) Evaluation of relative importance of compactional processes and cementation to porosity development of sandstone, according to Ehrenberg (1989) and Li *et al*. (2011).

perpendicular to the direction of the present stress field; the average aperture value (0.078 mm) of the N–S-aligned strike fracture is therefore the smallest (Fig. 13a). The filling degree of fractures is higher when the fracture angle becomes smaller, so the proportion of fully filled and partially filled fractures is the lowest among high-angle fractures (Fig. 13b). However, the fracture aperture does not increase with the rise of the dip angle, and the high values of fracture aperture are clustered between 30° and 60° (Fig. 13c). After formation, natural fractures experience the same diagenesis as the pores within the host rock matrix (Laubach, 2003) and the fracture aperture will be affected by compaction and cementation. In the Xinchang area, the effect of compaction on the tight reservoir is stronger than that of cementation (Fig. 13d). The vertical compaction greatly limits the aperture of near-horizontal and low-angle fractures, but has little effect on the middle-angle, high-angle and nearly vertical fractures. It is shown that the apertures of the near-horizontal and low-angle fractures have negative correlations with burial depth as a result of the vertical compaction (Fig. 14a), while there is no significant variation of the apertures of 30–90° fractures with burial depth (Fig. 14b, c). The lateral compaction caused by tectonic stress in foreland basin accounts for about 40% of the total pore reduction caused by compaction in tight reservoirs, while the rest of the pore reduction is caused by

vertical compaction (Shou *et al.* 2003; Gao *et al.* 2018). The influence of lateral compaction on fracture aperture therefore cannot be ignored. Located in the NW of the Sichuan foreland basin, the Longmen Mountain, as the provenance, continuously provides clastic matter to the basin. In the meantime, the lateral compaction in the NW direction caused by over-thrusting could reduce the aperture of high-angle or nearly vertical fractures; fractures with NE-aligned strike were influenced the most (Fig. 14d). On the other hand, the lateral structural compression in the NE direction had little influence on the nearly horizontal and low-angle fractures. In the study area, compaction has a significant effect on fracture apertures of 0–30° and 60–90°, but has little impact on fracture apertures of 30–60°. In conclusion, as a result of the combined effects of compaction and cementation, the seepage capacity of the fractures with dip angle > 30° is better than for a dip angle of 0–30° at present (Fig. 13c).

## 5.e. Effect of natural fractures on tight gas production capacity

According to the analysis of fractures within cores from nine vertical wells and their production data, the initial gas production of the vertical wells presents a positive correlation with the fracture
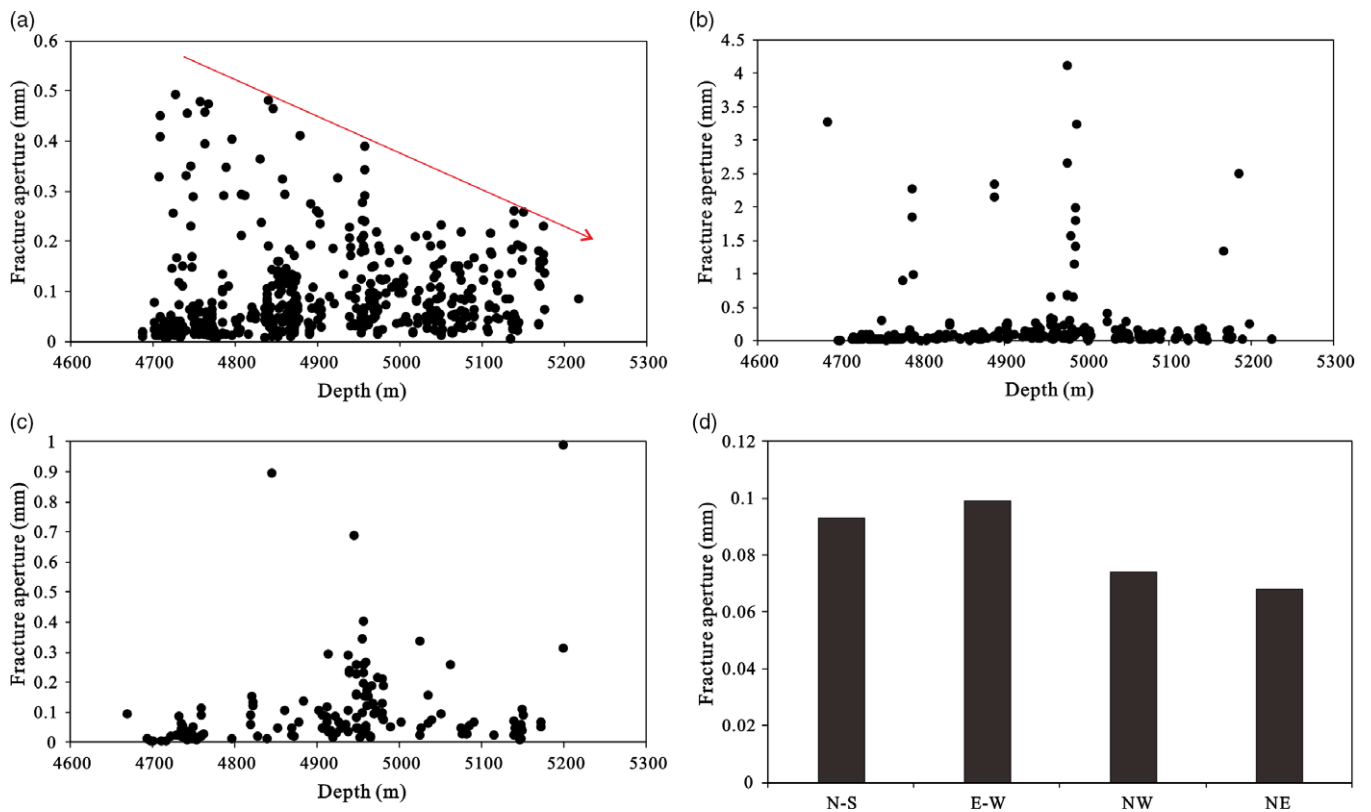
**Fig. 14.** (Colour online) The relationship between depth and fracture aperture in (a) the nearly horizontal fractures and low-angle fractures (0–30°); (b) middle-angle fractures (30–60°); and (c) the nearly vertical and high-angle fractures (60–90°). (d) The distribution of fracture aperture of fracture strike in the nearly vertical and high-angle fractures (60–90°).
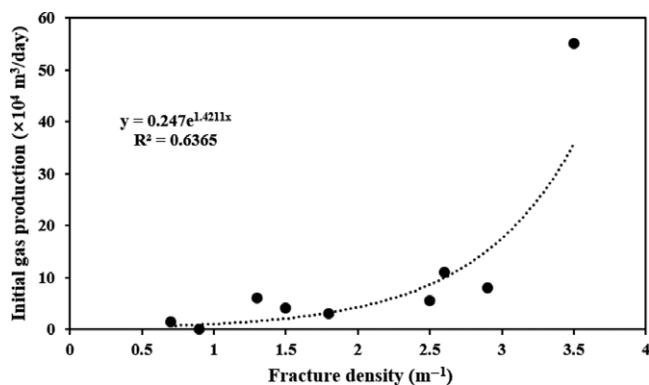


**Fig. 15.** The relationship between fracture density and initial gas production.

abundance ($R^2 = 0.6365$) (Fig. 15). This phenomenon is not related to whether the fractures are filled or not. The important material source of the calcite filling in the fractures is hydrocarbon, indicating that the fractures act as a tight gas migration channel before being filled. Due to the short-distance migration characteristics of tight gas and oil, it is possible for hydrocarbon to fill these fractures, providing a reliable source for high production. According to the production of tight gas in five typical tight gas production wells (Table 4), the productivity of individual wells can be divided into three categories: high (daily production > $20 \times 10^4$ m³/day), middle (daily production between $10 \times 10^4$ and $20 \times 10^4$ m³/day) and low (daily production < $10 \times 10^4$ m³/day). According

to the core observation, the high-productivity wells (Q11 and Q9) are dominated by fine sandstone and siltstone. This kind of lithology leads to an abundance of natural fractures (the fracture density is between 2.6 and 3.5 m$^{-1}$). The rocks with more brittle minerals (such as calcite and quartz), finer grain size and better assortment are easily fractured (Kong *et al.* 2018). For example, natural fractures in the siltstones are the most developed, followed by fine sandstones and medium sandstones (Gong *et al.* 2019*a*). The main strike of fractures in the well is consistent with the direction of the maximum principal stress (E–W), and the fractures with the dip angle between 30 and 90° are the majority (*c.* 46.94–66.67%). The fracture strike and dip angle jointly determine that the average apertures of the natural fractures in the samples from this well are the largest (with an average aperture of 0.077–0.082 mm). The content of fine sandstone and siltstone in middle-productivity well Q15 is medium, and the fracture strength is moderate (fracture density, 1.8 m$^{-1}$). The fractures are mainly in the E–W direction, and the fractures with the dip angle of 30–90° (*c.* 34.19%) are less frequent than in a high-productivity well; the average fracture aperture is 0.072 mm. The overall development strength and effectiveness of the fracture are also lower than that for the high-productivity well. Natural fractures therefore make a moderate contribution to the oil and gas production capacity. The lithology of cored samples from low-productivity well Q1 is complex so that the natural fractures can be rarely found there (the fracture density is 0.9 m$^{-1}$). The condition of low-productivity well Q5 is similar to that of Well Q1, with the lithology dominated by gritstone and medium sandstone. The main strike of fractures in the well is nearly NW and NE, with an average fracture aperture of

**Table 4.** The relationship between tight gas daily productivity and fracture attributes

| Well | Productivity types | Fracture density (m⁻¹) | Fracture aperture (mm) | Daily production (×10⁴ m³/day) | Fracture strike | The proportion of fractures angles of 30–90° (%) |
|------|-------------------|----------|----------|----------|---------|----------|
| Q11 | High | 3.5 | 0.082 | 56.9 | E–W | 66.67 |
| Q9 | High | 2.6 | 0.077 | 25.1 | E–W, N–S | 46.94 |
| Q15 | Middle | 1.8 | 0.072 | 17.7 | NE, E–W | 41.88 |
| Q5 | Low | 1.3 | 0.070 | 8.58 | NE, NW | 30.12 |
| Q1 | Low | 0.9 | 0.043 | 0.2 | NE, NW, N–S | 25.00 |

0.043 mm. The principal fracture strikes in low-productivity wells are not consistent with the maximum principal stress direction, and the fracture apertures are smaller than those in middle-productivity wells. The fracture strike and dip angle determine the fracture aperture, and the fracture aperture further determines the tight gas production of an individual well. In this study, the fractures apertures of wells Q9, Q15 and Q5 are regarded as approximately equal. However, there is a relatively huge disparity in their fracture density, and this decrease could also be ascribed to the decreasing content of fine sandstone and siltstone. These production characteristics indicate that the intensity of natural fractures could be the critical factor that influences initial gas production, and the effectiveness and intensity of natural fractures are the key factors for keeping the production of tight gas high and stable.

## 6. Conclusions

(1) The main natural fractures are tectonic fractures and diagenetic fractures, in which tectonic shear fracture and bedding fracture are the main types, respectively. There are four groups of dominant fractures: E–W, NE–SW, N–S and NW–SE strike.

(2) Three stages of tectonic fractures were formed during the late Indosinian, the middle and late Yanshanian, and the Himalayan periods, and two stages of bedding fractures were formed in the middle and late Indosinian and late Yanshanian periods. The primary bedding fracture and the second-stage tectonic fracture formed the early fracture network and determined the charging and short-distance migration of tight gas. The late fracture network system was formed by the reopening of bedding fractures and the third-stage tectonic fractures, enabling the adjustment and transformation of the original gas reservoir; the seepage ability of the tight reservoir was restored.

(3) The effectiveness of the natural fracture mainly depends on the direction of current maximum principal stress and the dip angle of the fractures. When fractures strike E–W and the dip angle is > 30°, the effectiveness of the fracture of the reservoir reaches its highest level. The development strength and aperture of natural fractures are the fundamental factors that determine the tight gas production.

## Reference

**Aguilera R** (1998) Geologic aspects of naturally fractured reservoirs. *Leading Edge* **17**, 1667.

**Ameen MS and Hailwood EA** (2008) A new technology for the characterization of microfractured reservoirs (test case: Unayzah reservoir, Wudayhi field, Saudi Arabia). *AAPG Bulletin* **92**, 31–52.

**Ameen MS, MacPherson K, Al-Marhoon MI and Rahim Z** (2012) Diverse fracture properties and their impact on performance in conventional and tight-gas reservoirs, Saudi Arabia: The Unayzah, South Haradh case study. *AAPG Bulletin* **96**, 459–92.

**Baron M, Parnell J, Mark D, Carr A, Przyjalgowski M and Feely M** (2008) Evolution of hydrocarbon migration style in a fractured reservoir deduced from fluid inclusion data, Clair Field, west of Shetland, UK. *Marine and Petroleum Geology* **25**, 153–72.

**Becker SP, Eichhubl P, Laubach SE, Reed RM, Lander RH and Bodnar RJ** (2010) A 48 m.y. history of fracture opening, temperature, and fluid pressure: Cretaceous Travis Peak Formation, East Texas basin. *Geological Society of America Bulletin* **122**, 1081–93.

**Brouste A, Renard F, Gratier JP and Schmittbuhl J** (2007) Variety of stylolites' morphologies and statistical characterization of the amount of heterogeneities in the rock. *Journal of Structural Geology* **29**, 422–34.

**Cao C** (2005) *Tectonic Stress Field and Application in the Northwest Sichuan Basin.* Beijing: Chinese Academy of Geological Science, pp. 39–43 (in Chinese with English abstract).

**Carey JW, Lei Z, Rougier E, Mori H and Viswanathan H** (2015) Fracture-permeability behavior of shale. *Journal of Unconventional Oil and Gas Resources* **11**, 27–43.

**Chen DX, Pang XQ, Yang KM, Yang Y and Ye J** (2012) Porosity evolution of tight gas sand of the second member of Xujiahe Formation of Upper Triassic, western Sichuan depression. *Journal of Jilin University (Earth Science Edition)* **42**(Supplement 1), 42–51 (in Chinese with English abstract).

**Chowdhury AH and Noble JPA** (1996) Origin, distribution and significance of carbonate cements in the Albert formation reservoir sandstones, New Brunswick, Canada. *Marine and Petroleum Geology* **13**, 837–46.

**Cuong TX and Warren JK** (2009) Bach ho field, a fractured granitic basement reservoir, Cuu Long Basin, offshore SE Vietnam: a 'buried-hill' play. *Journal of Petroleum Geology* **32**, 129–56.

**Dai J, Li J, Ding W, Hu G, Luo X, Hou L, Tao S, Zhang W and Zhu G** (2007) Geochemical characteristics of natural gas at giant accumulations in China. *Journal of Petroleum Geology* **30**, 275–88.

**de Graaf S, Reijmer JJG, Bertotti GV, Bezerra FHR, Cazarin CL, Bisdom K and Vonhof HB** (2017) Fracturing and calcite cementation controlling fluid flow in the shallow-water carbonates of the Jandaíra Formation, Brazil. *Marine and Petroleum Geology* **80**, 382–93.

**Deng H, Liu Y, Peng X, Liu Y and Li HA** (2018) A new index used to characterize the near-wellbore fracture network in naturally fractured gas reservoirs. *Journal of Natural Gas Science and Engineering* **55**, 52–63.

**Deng H, Zhou W, Zhou Q, Chen W and Zhang H** (2013) Quantification characterization of the valid natural fractures in the 2nd Xu Member, Xinchang gas field. *Acta Petrologica Sinica* **29**, 1087–97 (in Chinese with English abstract).

**Ding W, Wang X, Hu Q, Yin S, Cao X and Liu J** (2015) Progress in tight sand-stone reservoir fractures research. *Advances in Earth Science* **30**, 737–50 (in Chinese with English abstract).

**Ehrenberg SN** (1989) Assessing the relative importance of compaction processes and cementation to reduction of porosity in sandstones: discussion; compaction and porosity evolution of Pliocene Sandstones, Ventura Basin, California. *AAPG Bulletin* **73**, 1274–6.

**English JM and Laubach SE** (2017) Opening-mode fracture systems: insights from recent fluid inclusion microthermometry studies of crack-seal fracture cements. In *Geomechanics and Geology* (eds JP Turner, D Healy, RR Hillis and MJ Welch), pp. 257–72. Geological Society of London, Special Publication no. 458.

**Fall A, Eichhubl P, Bodnar RJ, Laubach SE and Steve Davis J** (2015) Natural hydraulic fracturing of tight-gas sandstone reservoirs, Piceance Basin, Colorado. *Geological Society of America Bulletin* **127**, 61–75.

**Fall A, Eichhubl P, Cumella SP, Bodnar RJ, Laubach SE and Becker SP** (2012) Testing the basin-centered gas accumulation model using fluid inclusion observations: Southern Piceance Basin, Colorado. *AAPG Bulletin* **96**, 2297–318.

**Fayek M, Harrison TM, Grove M, McKeegan KD, Coath CD and Boles JR** (2001) In situ stable isotopic evidence for protracted and complex carbonate cementation in a petroleum reservoir, North Coles levee, San Joaquin basin, California, USA. *Journal of Sedimentary Research* **71**, 444–58.

**Felici F, Alemanni A, Bouacida D and de Montleau P** (2016) Fractured reservoir modeling: from well data to dynamic flow. Methodology and application to a real case study in Illizi Basin (Algeria). *Tectonophysics* **690**, 117–30.

**Friedman I and O'Neil JR** (1977) Compilation of Stable Isotope Fractionation Factors of Geochemical Interest. *USGS Professional Paper* **44-K**, 11 pp.

**Gale JFW, Laubach SE, Olson JE, Eichhubl P and Fall A** (2017) Natural fractures in shale: a review and new observations. *AAPG Bulletin* **101**, 2165–216.

**Gao J, He S, Zhao JX and Yi J** (2017) Geothermometry and geobarometry of overpressured lower Paleozoic gas shales in the Jiaoshiba field, Central China: insight from fluid inclusions in fracture cements. *Marine and Petroleum Geology* **83**, 124–39.

**Gao Z, Ma J, Cui J, Feng J, Zhou C and Wu H** (2018) Deep reservoir pore evolution model of a geological process from burial compaction to lateral extrusion. *Acta Petrologica Sinica* **36**, 176–87 (in Chinese with English abstract).

**Gasparrini M, Lacombe O, Rohais S, Belkacemi M and Euzen T** (2021) Natural mineralized fractures from the Montney-Doig unconventional reservoirs (Western Canada Sedimentary Basin): timing and controlling factors. *Marine and Petroleum Geology* **124**, 104826.

**Gong L, Fu X, Wang Z, Gao S, Jabbari H, Yue W and Liu B** (2019a) A new approach for characterization and prediction of natural fracture occurrence in tight oil sandstones with intense anisotropy. *AAPG Bulletin* **103**, 1383–400.

**Gong L, Su X, Gao S, Fu X, Jabbari H, Wang X, Liu B, Yue W, Wang Z and Gao A** (2019b) Characteristics and formation mechanism of natural fractures in the tight gas sandstones of Jiulongshan gas field, China. *Journal of Petroleum Science and Engineering* **175**, 1112–21.

**Guo Y, Pang X, Chen D, Leng J and Tian J** (2012) Evolution of continental formation pressure in the middle part of the Western Sichuan Depression and its significance on hydrocarbon accumulation. *Petroleum Exploration and Development* **39**, 457–65.

**Halihan T, Mace RE and Sharp J** (2000) Flow in the San Antonio segment of the Edwards aquifer: matrix, fractures, or conduits? In *Groundwater Flow and Contaminant Transport in Carbonate Aquifers* (eds ID Sasowsky and CM Wicks), pp. 129–46. Rotterdam, Netherlands: AA Balkema.

**Hennig GJ and Grün R** (1983) ESR dating in quaternary geology. *Quaternary Science Reviews* **2**, 157–238.

**Henriksen H and Braathen A** (2006) Effects of fracture lineaments and in-situ rock stresses on groundwater flow in hard rocks: a case study from Sunnfjord, western Norway. *Hydrogeology Journal* **14**, 444–61.

**Higgs KE, Zwingmann H, Reyes AG and Funnell RH** (2007) Diagenesis, porosity evolution, and petroleum emplacement in tight gas reservoirs, Taranaki Basin, New Zealand. *Journal of Sedimentary Research* **77**, 1003–25.

**Hooker JN, Gale JFW, Gomez LA, Laubach SE, Marrett R and Reed RM** (2009) Aperture-size scaling variations in a low-strain opening-mode fracture set, Cozzette Sandstone, Colorado. *Journal of Structural Geology* **31**, 707–18.

**Hooker JN, Larson TE, Eakin A, Laubach SE, Eichhubl P, Fall A and Marrett R** (2015) Fracturing and fluid flow in a sub-décollement sandstone; or, a leak in the basement. *Journal of the Geological Society* **172**, 428–42.

**Huang P** (1994) Study on electron spin resonance (ESR) dating of fault movement. *Seismology & Geology* **16**, 269–74.

**Irwin H, Curtis C and Coleman M** (1977) Isotopic evidence for source of diagenetic carbonates formed during burial of organic-rich sediments. *Nature* **269**, 209–13.

**Jin W, Tang L, Yang K, Wan G and Lü Z** (2010) Segmentation of the Longmen Mountains thrust belt, Western Sichuan Foreland Basin, SW China. *Tectonophysics* **485**, 107–21.

**Kanjanapayont P, Aydin A, Wongseekaew K and Maneelok W** (2016) Structural characterization of the fracture systems in the porcelanites: comparing data from the Monterey Formation in California USA and the Sap Bon Formation in Central Thailand. *Journal of Structural Geology* **90**, 177–84.

**Kong L, Ostadhassan M, Li C and Tamimi N** (2018) Pore characterization of 3D-printed gypsum rocks: a comprehensive approach. *Journal of Materials Science* **53**, 5063–78.

**Lai J, Wang G, Fan Z, Chen J, Qin Z, Xiao C, Wang S and Fan X** (2017) Three-dimensional quantitative fracture analysis of tight gas sandstones using industrial computed tomography. *Scientific Reports* **7**, 1825.

**Lander RH and Laubach SE** (2014) Insights into rates of fracture growth and sealing from a model for quartz cementation in fractured sandstones. *Geological Society of America Bulletin* **127**, 516–38.

**Laubach SE** (1988) Subsurface fractures and their relationship to stress history in East Texas basin sandstone. *Tectonophysics* **156**, 37–49.

**Laubach SE** (2003) Practical approaches to identifying sealed and open fractures. *AAPG Bulletin* **87**, 561–79.

**Laubach SE, Eichhubl P, Hilgers C and Lander RH** (2010) Structural diagenesis. *Journal of Structural Geology* **32**, 1866–72.

**Laubach SE, Lander RH, Criscenti LJ, Anovitz LM, Urai JL, Pollyea RM, Hooker JN, Narr W, Evans MA, Kerisit SN, Olson JE, Dewers T, Fisher D, Bodnar R, Evans B, Dove P, Bonnell LM, Marder MP and Pyrak-Nolte L** (2019) The role of chemistry in fracture pattern development and opportunities to advance interpretations of geological materials. *Reviews of Geophysics* **57**(3), 1065–111.

**Laubach SE and Ward ME** (2006) Diagenesis in porosity evolution of opening-mode fractures, Middle Triassic to Lower Jurassic La Boca Formation, NE Mexico. *Tectonophysics* **419**, 75–97.

**Lavenu APC, Lamarche J, Salardon R, Gallois A, Marié L and Gauthier BDM** (2014) Relating background fractures to diagenesis and rock physical properties in a platform-slope transect. Example of the Maiella Mountain (central Italy). *Marine and Petroleum Geology* **51**, 2–19.

**Law BE and Curtis JB** (2002) Introduction to unconventional petroleum systems. *AAPG Bulletin* **86**, 1851–2.

**Leng J, Li S and Yang C** (2011) Determination of the time of gas accumulation in the Xujiahe Formation of Xiaoquan-Fenggu structural belt in the Western Sichuan Depression through fluid inclusion analysis. *Natural Gas Industry* **31**, 38–42.

**Lézin C, Odonne F, Massonnat GJ and Escadeillas G** (2009) Dependence of joint spacing on rock properties in carbonate strata. *AAPG Bulletin* **93**, 271–90.

**Li C, Zhao L, Liu B, Liu H, Li J, Fan Z, Wang J, Li W, Zhao W and Sun M** (2021) Origin, distribution and implications on production of bedding-parallel fractures: a case study from the Carboniferous KT-I formation in the NT oilfield, Precaspian Basin, Kazakhstan. *Journal of Petroleum Science and Engineering* **196**, 107655.

**Li M, Zhu R, Lou Z, Yin W, Hu Z, Zhu H and Jin A** (2019) Diagenesis and its impact on the reservoir quality of the fourth member of Xujiahe Formation, Western Sichuan Depression, China. *Marine and Petroleum Geology* **103**, 485–98.

**Li R, Lyu ZX and Ye SJ** (2011) Impact of diagenesis on reservoir-quality evolution in the Upper Triassic Xujiahe tight sandstones. West Sichuan, China. *Journal of Chengdu University of Technology (Science and Technology Edition)* **38**, 147–55 (in Chinese with English abstract).

**Li Z, Jia D, Chen W, Yin H, Shen L, Sun C, Zhang Y, Li Y, Li S, Zhou X, Li H, Jian G, Zhang M and Cui J** (2014) Late Cenozoic east-west crustal shortening in southern Longmen Shan, eastern Tibet: implications for regional stress field changes. *Tectonophysics* **623**, 169–86.

**Liang H, Xu F, Xu G, Yuan H, Huang S, Wang Y, Wang L and Fu D** (2019) Geochemical characteristics and origins of the diagenetic fluids of the Permian Changxing Formation calcites in the Southeastern Sichuan Basin: evidence from petrography, inclusions and Sr, C and O isotopes. *Marine and Petroleum Geology* **103**, 564–80.

**Liang X and Gao J** (1999) Study on the α-quartz dating of fault-related ore mineralization. *Journal of Mineralogy and Petrology* **19**, 69–71 (in Chinese with English abstract).

**Liu D, Zhang C, Pan Z, Huang Z, Luo Q, Song Y and Jiang Z** (2020) Natural fractures in carbonate-rich tight oil reservoirs from the Permian Lucaogou Formation, southern Junggar Basin, NW China: insights from fluid inclusion microthermometry and isotopic geochemistry. *Marine and Petroleum Geology* **119**, 104500.

**Liu K, Bourdet J, Zhang B, Zhang N, Lu X, Liu S, Pang H, Li Z and Guo X** (2013) Hydrocarbon charge history of the Tazhong Ordovician reservoirs, Tarim Basin as revealed from an integrated fluid inclusion study. *Petroleum Exploration and Development* **40**, 171–80.

**Liu SB, Huang SJ, Shen ZM, Lü ZX and Song RC** (2014) Diagenetic fluid evolution and water-rock interaction model of carbonate cements in sandstone: an example from the reservoir sandstone of the Fourth Member of the Xujiahe Formation of the Xiaoquan-Fenggu area, Sichuan Province, China. *Science China Earth Sciences* **57**, 1077–92.

**Liu SB, Shen ZM, Lu ZX and Luo XP** (2009) Research on the geochronology of forming the gas pools of Member 2 of Xujiahe Formation in the middle West Sichuan depression, China. *Journal of Chengdu University of Technology (Science and Technology Edition)* **36**, 523–30 (in Chinese with English abstract).

**Liu Y, Chen D, Qiu N, Fu J and Jia J** (2018a) Geochemistry and origin of continental natural gas in the western Sichuan basin, China. *Journal of Natural Gas Science and Engineering* **49**, 123–31.

**Liu Y, Hu W, Cao J, Wang X, Tang Q, Wu H and Kang X** (2018b) Diagenetic constraints on the heterogeneity of tight sandstone reservoirs: a case study on the Upper Triassic Xujiahe Formation in the Sichuan Basin, southwest China. *Marine and Petroleum Geology* **92**, 650–69.

**Liu Y, Hu W, Cao J, Wang X, Zhu F, Tang Q and Gao W** (2019) Fluid–rock interaction and its effects on the Upper Triassic tight sandstones in the Sichuan Basin, China: insights from petrographic and geochemical study of carbonate cements. *Sedimentary Geology* **383**, 121–35.

**Luo L** (2015) *Research on Diagenetic Facies of the 2nd Member of Xujiahe Formation in the Xinchang Structural Belt*. Chengdu: Chengdu University of Technology (in Chinese with English abstract).

**Luo L, Meng W, Gluyas J, Tan X, Gao X, Feng M, Kong X and Shao H** (2019) Diagenetic characteristics, evolution, controlling factors of diagenetic system and their impacts on reservoir quality in tight deltaic sandstones: typical example from the Xujiahe Formation in Western Sichuan Foreland Basin, SW China. *Marine and Petroleum Geology* **103**, 231–54.

**Luthi SM and Souhaité P** (1990) Fracture apertures from electrical borehole scans. *Geophysics* **55**, 821–33.

**Lyu W, Zeng L, Zhang B, Miao F, Lyu P and Dong S** (2017) Influence of natural fractures on gas accumulation in the Upper Triassic tight gas sandstones in the northwestern Sichuan Basin, China. *Marine and Petroleum Geology* **83**, 60–72.

**Ma X, Zhou W, Tang Y, Deng H, Lei T and Wang J** (2013) Timing of natural fractures formed in the gas reservoirs of the 2nd member of Xujiahe Fm in the Xinchang area, western Sichuan Basin. *Natural Gas Industry* **33**, 15–19 (in Chinese with English abstract).

**Mack GH, Cole DR, Giordano TH, Schaal WC and Barcelos JH** (1991) Paleoclimatic controls on stable oxygen and carbon isotopes in caliche of the Abo Formation (Permian), south-central New Mexico, USA. *Journal of Sedimentary Petrology* **61**, 458–72.

**Maillot J, Davy P, Le Goc R, Darcel C and de Dreuzy JR** (2016) Connectivity, permeability, and channeling in randomly distributed and kinematically defined discrete fracture network models. *Water Resources Research* **52**, 8526–45.

**Morad S, Al-Aasm IS, Ramseyer K, Marfil R and Aldahan AA** (1990) Diagenesis of carbonate cements in Permo-Triassic sandstones from the Iberian Range, Spain: evidence from chemical composition and stable isotopes. *Sedimentary Geology* **67**, 281–95.

**Olson JE, Laubach SE and Lander RH** (2009) Natural fracture characterization in tight gas sandstones: integrating mechanics and diagenesis. *AAPG Bulletin* **93**, 1535–49.

**Osborne M and Haszeldine S** (1993) Evidence for resetting of fluid inclusion temperatures from quartz cements in oilfields. *Marine and Petroleum Geology* **10**, 271–8.

**Pang X, Peng J, Jiang Z, Yang H, Wang P, Jiang F and Wang K** (2019) Hydrocarbon accumulation processes and mechanisms in Lower Jurassic tight sandstone reservoirs in the Kuqa subbasin, Tarim Basin, northwest China: a case study of the Dibei tight gas field. *AAPG Bulletin* **103**, 769–96.

**Pecher A** (1981) Experimental decrepitation and re-equilibration of fluid inclusions in synthetic quartz. *Tectonophysics* **78**, 567–83.

**Peng Z, Yuan W, Li P and Man F** (1993) Preliminary study on errors in ESR age estimate. *Nuclear Techniques* **16**, 200–03 (in Chinese with English abstract).

**Petrie ES, Evans JP and Bauer SJ** (2014) Failure of cap-rock seals as determined from mechanical stratigraphy, stress history, and tensile-failure analysis of exhumed analogs. *AAPG Bulletin* **98**, 2365–90.

**Ponziani M, Slob E, Luthi S, Bloemenkamp R and Le Nir I** (2015) Experimental validation of fracture aperture determination from borehole electric microresistivity measurements. *Geophysics* **80**, D175–81.

**Qin S, Zhang Y, Zhao C and Zhou Z** (2018) Geochemical evidence for in situ accumulation of tight gas in the Xujiahe Formation coal measures in the central Sichuan Basin, China. *International Journal of Coal Geology* **196**, 173–84.

**Qiu D, Liu Q, Yun J, Jin Z, Zhu D, Li T and Sun D** (2018) Electron spin resonance (ESR) dating of pre-Quaternary faults in the Sichuan basin, SW China. *Journal of Asian Earth Sciences* **163**, 142–51.

**Ren S, Song C and Li J** (2016) Application of electron spin resonance (ESR) dating to ductile shearing: examples from the Qinling orogenic belt, China. *Journal of Structural Geology* **85**, 12–7.

**Sanderson DJ, Roberts S and Gumiel P** (1994) A fractal relationship between vein thickness and gold grade in drill core from La Codosera, Spain. *Economic Geology* **89**, 168–73.

**Schmoker JW** (1996) A resource evaluation of the Bakken Formation (Upper Devonian and Lower Mississippian) continuous oil accumulation, Williston Basin, North Dakota and Montana. *Mountain Geologist* **33**, 1–10.

**Shi J, Zeng L, Zhao X, Zhang Y and Wang J** (2020) Characteristics of natural fractures in the upper Paleozoic coal bearing strata in the southern Qinshui Basin, China: implications for coalbed methane (CBM) development. *Marine and Petroleum Geology* **113**, 104152.

**Shou J, Zhu G and Zhang H** (2003) Lateral structure compression and its influence on sandstone diagenesis: a case study from the Tarim Basin. *Acta Sedimentol Sinica* **21**, 90–5 (in Chinese with English abstract).

**Solano N, Zambrano L and Aguilera R** (2011) Cumulative-gas-production distribution on the nikanassin tight gas formation, alberta and British Columbia, Canada. *SPE Reservoir Evaluation and Engineering* **14**, 357–76.

**Spero HJ, Bijma J, Lea DW and Bernis BE** (1997) Effect of seawater carbonate concentration on foraminiferal carbon and oxygen isotopes. *Nature* **390**, 497–500.

**Spötl C and Wright VP** (1992) Groundwater dolocretes from the Upper Triassic of the Paris Basin, France: a case study of an arid, continental diagenetic facies. *Sedimentology* **39**(6), 1119–36.

**Tao S, Zou C, Mi J, Gao X, Yang C, Zhang X and Fan J** (2014) Geochemical comparison between gas in fluid inclusions and gas produced from the Upper Triassic Xujiahe Formation, Sichuan Basin, SW China. *Organic Geochemistry* **74**, 59–65.

**Tsakalos E, Kazantzaki M, Lin A, Bassiakos Y, Filippaki E and Takafumi N** (2018) Seismic moment and recurrence: microstructural and mineralogical characterization of rocks in carbonate fault zones and their potential for luminescence and ESR dating. *Journal of Structural Geology* **117**, 186–202.

**Ukar E and Laubach SE** (2016) Syn- and postkinematic cement textures in fractured carbonate rocks: insights from advanced cathodoluminescence imaging. *Tectonophysics* **690**, 190–205.

**Ulrich MR and Bodnar RJ** (1988) Systematics of stretching of fluid inclusions II: barite at 1 atm confining pressure. *Economic Geology* 83, 1037–46.

**Voinchet P, Yin G, Falguères C, Liu C, Han F, Sun X and Bahain JJ** (2019) Dating of the stepped quaternary fluvial terrace system of the Yellow River by electron spin resonance (ESR). *Quaternary Geochronology* 49, 278–82.

**Wang Q, Chen D, Gao X, Wang F, Li J, Liao W, Wang Z and Xie G** (2020) Microscopic pore structures of tight sandstone reservoirs and their diagenetic controls: a case study of the Upper Triassic Xujiahe Formation of the Western Sichuan Depression, China. *Marine and Petroleum Geology* 113.

**Wang Q, Laubach SE and Fall A** (2019) Coupled effects of diagenesis and deformation on fracture evolution in deeply buried sandstones. In Proceedings of 53rd US Rock Mechanics/Geomechanics Symposium. 23–26 June 2019, New York. American Rock Mechanics Association.

**Wang Q, Laubach SE, Gale JFW and Ramos MJ** (2019) Quantified fracture (joint) clustering in Archean basement, Wyoming: application of the normalized correlation count method. *Petroleum Geoscience* 25, 415–28.

**Wang Q, Narr W and Laubach S** (2020) Characterizing subsurface fracture spatial distribution in the East Painter Reservoir Anticline, Wyoming. In *Proceedings of Virtual SPE/AAPG/SEG Unconventional Resources Technology Conference.* 20–22 July 2020.

**Watson EB and Brenan JM** (1987) Fluids in the lithosphere, 1. Experimentally-determined wetting characteristics of $CO_2H_2O$ fluids and their implications for fluid transport, host-rock physical properties, and fluid inclusion formation. *Earth and Planetary Science Letters* 85, 497–515.

**Wei W, Zhu X, Tan M, Xue M, Guo D, Su H and Wang P** (2015) Diagenetic and porosity evolution of conglomerate sandstones in Bayingebi Formation of the Lower Cretaceous, Chagan Sag, China-Mongolia frontier area. *Marine and Petroleum Geology* 66, 998–1012.

**Wu H, Hu W, Tang Y, Cao J, Wang X, Wang Y and Kang X** (2017) The impact of organic fluids on the carbon isotopic compositions of carbonate-rich reservoirs: case study of the Lucaogou Formation in the Jimusaer Sag, Junggar Basin, NW China. *Marine and Petroleum Geology* 85, 136–50.

**Xi K, Cao Y, Jahren J, Zhu R, Bjørlykke K, Haile BG, Zheng L and Hellevang H** (2015) Diagenesis and reservoir quality of the Lower Cretaceous Quantou Formation tight sandstones in the southern Songliao Basin, China. *Sedimentary Geology* 330, 90–107.

**Xu C, Gehenn JM, Zhao D, Xie G and Teng MK** (2015) The fluvial and lacustrine sedimentary systems and stratigraphic correlation in the Upper Triassic Xujiahe Formation in Sichuan Basin, China. *AAPG Bulletin* 99, 2023–41.

**Yang K, Zhu H, Ye J, Zhang K and Ke G** (2012) *The Geological Characteristics of Tight Sandstone Gas Reservoirs in West Sichuan Basin.* Beijing: Science Press.

**Yilmaz K, Umul B, Davis J and Nilson G** (2016) Tight gas development in the Mezardere Formation, Thrace Basin Turkey. *Journal of Natural Gas Science and Engineering* 33, 551–61.

**Yu Y, Lin L, Zhai C, Chen H, Wang Y, Li Y and Deng X** (2019) Impacts of lithologic characteristics and diagenesis on reservoir quality of the 4th member of the Upper Triassic Xujiahe Formation tight gas sandstones in the western Sichuan Basin, southwest China. *Marine and Petroleum Geology* 107, 1–19.

**Yue D, Wu S, Xu Z, Xiong L, Chen D, Ji Y and Zhou Y** (2018) Reservoir quality, natural fractures, and gas productivity of upper Triassic Xujiahe tight gas sandstones in western Sichuan Basin, China. *Marine and Petroleum Geology* 89, 370–86.

**Zeng L** (2010) Microfracturing in the Upper Triassic Sichuan Basin tight-gas sandstones: tectonic, overpressure, and diagenetic origins. *AAPG Bulletin* 94, 1811–25.

**Zeng L, Gong L, Zu K, Tang X, Wang T, Wang C and Xu W** (2012a) Influence factors on fracture validity of the Paleogene reservoir, Western Qaidam Basin. *Acta Geologica Sinica* 86, 1809–14 (in Chinese with English abstract).

**Zeng L, Jiang J and Yang Y** (2010a) Fractures in the low porosity and ultra-low permeability glutenite reservoirs: a case study of the late Eocene Hetaoyuan formation in the Anpeng Oilfield, Nanxiang Basin, China. *Marine and Petroleum Geology* 27, 1642–50.

**Zeng L, Ke S and Liu Y** (2010b) *Fracture Study Methods for Low Permeability Oil and Gas Reservoir.* Beijing: Petroleum Industry Press, pp. 32–35.

**Zeng L and Li X** (2009) Fractures in sandstone reservoirs with ultra-low permeability: a case study of the Upper Triassic Yanchang Formation in the Ordos Basin, China. *AAPG Bulletin* 93, 461–77.

**Zeng L and Liu H** (2009) The key geological factors influencing on development of low-permeability sandstone reservoirs: a case study of the Taizhao area in the Songliao Basin, China. *Energy Exploration & Exploitation* 27, 425–37.

**Zeng L, Tang X, Wang T and Gong L** (2012b) The influence of fracture cements in tight Paleogene saline lacustrine carbonate reservoirs, western Qaidam Basin,northwest China. *AAPG Bulletin* 96, 2003–17.

**Zeng L, Zhu R, Gao Z, Gong L and Liu G** (2016) Structural diagenesis and its petroleum geological significance. *Petroleum Science Bulletin* 1, 191–7.

**Zhang C, Zhu D, Luo Q, Liu L, Liu D, Yan L and Zhang Y** (2017) Major factors controlling fracture development in the Middle Permian Lucaogou Formation tight oil reservoir, Junggar Basin, NW China. *Journal of Asian Earth Sciences* 146, 279–95.

**Zhang G** (2005) Characteristics of fractures in the tight sandstone reservoirs of Xujiahe Formation in West Sichuan depression. *Natural Gas Industry* 25, 11–3 (in Chinese with English abstract).

**Zhang L, Guo X, Hao F, Zou H and Li P** (2016) Lithologic characteristics and diagenesis of the Upper Triassic Xujiahe Formation, Yuanba area, northeastern Sichuan Basin. *Journal of Natural Gas Science and Engineering* 35, 1320–35.

**Zhang S, Li D, Deng L and Liu C** (1995) Application of ESR dating technique to fractured reservoir. *Journal of Chengdu Institute of Technology* 22, 7–11 (in Chinese with English abstract).

**Zhang Y, Zeng L, Luo Q, Zhu R, Pan S, Dai Q, Shi J, Qin J and Xu X** (2020) Effects of diagenesis on natural fractures in tight oil reservoirs: a case study of the Permian Lucaogou Formation in Jimusar Sag, Junggar Basin, NW China. *Geological Journal* 55, 6562–79.

**Zhang YZ, Zeng L, Luo Q, Zhang C, Wu H, Lyu W, Dai Q and Zhu D** (2018) Research on the types and genetic mechanisms of tight reservoir in the Lucaogou Formation in Jimusar Sag, Junggar Basin. *Natural Gas Geoscience* 29, 211–25 (in Chinese with English abstract).

**Zhao W, Bian C, Xu C, Wang H, Wang T and Shi Z** (2011) Assessment on gas accumulation potential and favorable plays within the Xu-1, 3 and 5 Members of the Xujiahe Formation in the Sichuan Basin. *Petroleum Exploration and Development* 38, 385–93.

**Zhao X, Hu X, Zeng L, Xiao K, Li H, You Y and Feng Q** (2017) Evaluation on the effectiveness of natural fractures in Changxing Fm reef-flat facies reservoirs, Yuanba area, Sichuan Basin. *Natural Gas Industry B* 4, 239–48 (in Chinese with English abstract).

**Zheng D, Pang X, Ma X, Li C, Zheng T and Zhou L** (2019) Hydrocarbon generation and expulsion characteristics of the source rocks in the third member of the Upper Triassic Xujiahe Formation and its effect on conventional and unconventional hydrocarbon resource potential in the Sichuan Basin. *Marine and Petroleum Geology* 109, 175–92.

**Zou C, Dong D, Wang S, Li J, Li X, Wang Y, Li D and Cheng K** (2010) Geological characteristics and resource potential of shale gas in China. *Petroleum Exploration and Development* 37, 641–53.

**Zou C, Tao S, Zhu R, Yuan X, Li W, Zhang G, Zhang X, Gao X, Liu L, Xu C, Song J and Li G** (2009) Formation and distribution of 'continuous' gas reservoirs and their giant gas province: a case from the Upper Triassic Xujiahe Formation giant gas province, Sichuan Basin. *Petroleum Exploration and Development* 36, 307–19.

**Zou C, Yang Z, Zhu R, Wu S, Fu J, Lei D, Hou L, Lin S and Pan S** (2019) Geologic significance and optimization technique of sweet spots in unconventional shale systems. *Journal of Asian Earth Sciences* 178, 3–19.

**Zou CN, Yang Z, Tao SZ, Yuan XJ, Zhu RK, Hou LH, Wu ST, Sun L, Zhang GS, Bai B, Wang L, Gao XH and Pang ZL** (2013) Continuous hydrocarbon accumulation over a large area as a distinguishing characteristic of unconventional petroleum: the Ordos Basin, North-Central China. *Earth-Science Reviews* 126, 358–69.